Contrib Mineral Petrol (2003) 144: 739–757
DOI 10.1007/s00410-002-0426-x

ORIGINAL PAPER

Joseph M. Evensen · David London

Experimental partitioning of Be, Cs, and other trace elements between cordierite and felsic melt, and the chemical signature of S-type granite

Received: 14 March 2001 / Accepted: 14 October 2002 / Published online: 28 January 2003

Abstract The trace-element signature that cordierite (Crd) imparts to silicic magmas was evaluated by experiment using metapelite mineral mixtures to produce cordierite-bearing peraluminous granitic melts at 200 MPa (P_{H2O}), from 700 to 850 °C. Most elemental partition coefficients vary with T. Beryllium is strongly compatible, with $D_{Be}^{Crd/melt}$ values decreasing linearly from 202.0 to 6.7 as T rises from 700 to 850 °C. Manganese is compatible ($D_{Mn}^{Crd/melt} = 7.67$ to 1.92 over the same range of T), and shows similar values to those reported for biotite in silicic melts. Incompatible components include Li, Rb, B, F and P, although Cs is nearly compatible in cordierite, especially at higher T ($D_{Cs}^{Crd/melt} = \sim 0.19$ to 0.60) where the large alkalis are better accommodated structurally. Cordierite appears to be the most effective crystalline reservoir of Be and Cs in metapelites and their anatectic melts. Natural data support the hypothesis that Crd, when present in granitic melts, sequesters Be, Cs and, in the absence of garnet, Mn. S-type granitic rocks containing Crd show consistently low Be contents (mean = 0.8 ppm Be with an average range of < 1 to 1.20) whereas Crd-free granites (e.g., containing accessory garnet) exhibit distinctly higher Be contents (mean = 6 ppm Be with an average range of 3 to 12). These values increase further in evolved facies (mean = 69 ppm Be with a an average range of 11 to 145) which commonly give rise to beryl-bearing pegmatites. Whole-rock signatures of Be discriminate source environments of silicic magmas at a resolution equal to the boundaries of the cordierite stability field – e.g., at the P–T–X conditions where cordierite gives rise to garnet + aluminum silicate. Cordierite-bearing granitic rocks contain low Cs contents (mean = 1.8 ppm Cs) compared to the Crd-free equivalents (mean = 18 ppm Cs). Mn contents also correlate with the presence (mean = 0.01 wt% MnO) or absence of Crd (mean = 0.09 wt% MnO). Depending on its contribution to anatexis, cordierite may either *give* or *take* S-type chemical character from granitic liquids, resulting in a distinctive Crd-associated group of S-type elements. This signature is different from that of micas (high Li, F and, to a lesser degree, Be and Mn). Whole-rock compositions of granites, coupled with notable absences of beryl in their associated pegmatites, indicate that a sizable population of S-type granites originated from Crd-bearing sources. The normative Crd component of silicic peraluminous melts is ≤ 4 wt% to 850 °C. Higher modal contents of cordierite reflect either restite entrainment or peritectic reactions which produce Crd after magma ascent to shallow depths. The distinctive trace-element signature of cordierite now provides improved resolution of the source mineralogy for S-type magmas.

J.M. Evensen (✉) · D. London
School of Geology & Geophysics, University of Oklahoma,
100 East Boyd Street, Norman, Oklahoma 73019, USA
E-mail: joey.evensen@exxonmobil.com
Tel.: +1-713-4314939
Fax: +1-713-4316310

Present address: J.M. Evensen
ExxonMobil Upstream Research Company,
P.O. Box 2189, Houston, TX 77252, USA

Editorial responsibility: W. Schreyer

Introduction

Although the Be contents of rock-forming minerals are normally very low (Grew 2002), natural cordierite (Crd) can contain wt% levels of BeO (e.g., Schreyer et al. 1979; Gordillo et al. 1985). This observation revealed that the presence or absence of cordierite may largely determine the budget of Be in granitic rocks (Evensen and London 2002; London and Evensen 2002). Cordierite is a diagnostic phase in granites and rhyolites that originate from metasedimentary sources (the S-types: Chappell and White 1974), but peraluminous granitic rocks that contain garnet in addition to other peraluminous minerals are also common (e.g., Miller and Bradfish 1980). Because cordierite plays such an important role in

regulating Be, we present here the partition coefficients for Be and other normally trace lithophile elements between Crd and peraluminous silicic melt at 200 MPa (P_{H2O}), from 700 to 850 °C. With these data, we can assess how Crd influences the trace-element signature of peraluminous silicic melts (e.g., London 1995; Bea 1996; Chappell 1999) which lacked Crd throughout their evolution from those peraluminous granites and rhyolites that originated from Crd-bearing sources – even if all vestiges of Crd have been removed by restite unmixing, peritectic reactions, or obliterated by retrograde alteration.

Cordierite is found in metapelites and aluminous gneisses formed at relatively low pressures. The stability of Crd increases with Mg content to terminal reactions (mainly Crd = Gt + Als + Qtz + V) at pressures greater than ~600 to ~500 MPa from 650 to 900 °C (e.g., Hensen and Green 1973; Vielzeuf and Holloway 1988; Spear and Cheney 1989; Mukhopadhyay and Holdaway 1994). Cordierite may be a product of melting reactions (e.g., Clemens and Wall 1988; Pereira and Bea 1994; Carrington and Harley 1995) and commonly remains behind in restitic assemblages (e.g., Gordillo 1979; Ugidos 1988, 1990; Ugidos and Recio 1993; Bea et al. 1994a; Harley 1994; Kamber et al. 1998; Kriegsman and Hensen 1998; Kalt et al. 1999). Many Crd-bearing leucogranites apparently also contained Crd in their restite (e.g., Bea et al. 1994a). Peraluminous silicic magmas derived by anatexis of mixed metapelitic-quartzofeldspathic protoliths fractionate toward more peraluminous minimum melts (London 1995). Thus, cordierite may appear late in the evolution of mildly peraluminous granites (e.g., Morgan et al. 1998). Cordierite in granites may be replaced or superceded by tourmaline (Wolf and London 1997), or it may be altered beyond recognition by the common, fine-grained or symplectic intergrowths of chlorite, muscovite, and biotite.

Experimental methods

Starting materials

Starting compositions reflect source-rock assemblages with garnet + biotite as dominant ferromagnesian silicates, which yield mildly to moderately peraluminous silicic melts. Beryllium was not added explicitly, only by way of trace quantities which naturally exist in added white mica.

A subset of the starting mixtures and cordierite-producing reactions used by Evensen (2001) was utilized for Crd synthesis. Composite powders were formulated by combining mineral additives (Table 1) with a large fraction of a pelitic mineral mixture (designated "SPC"; Wolf and London 1997) to yield the weight fraction formulae $Ab_{22.7}Or_{9.6}Qtz_{26.6}Mus_{13.1}Bt_{12.3}Gt\text{-}1_{15.7}$ and $Ab_{25.5}Or_{10.8}Qtz_{29.0}Mus_{14.8}$ $Bt_{11.0}Gt\text{-}2_{8.0}$. Final experimental charges contained a slight excess of doubly distilled deionized water needed to saturate any melt created at 200 MPa and in the T range investigated (~10 wt% H_2O).

At 200 MPa (P_{H2O}) and in the presence of biotite, nucleation and growth of cordierite was achieved via the reaction:

$$\underset{\text{garnet}}{2(Mg,Fe)_3Al_2Si_3O_{12}} + \underset{\text{aluminumsilicate}}{4Al_2SiO_5} + \underset{\text{quartz}}{5SiO_2} = \underset{\text{cordierite}}{3(Mg,Fe)_2Al_4Si_5O_{18}} \quad (1)$$

in which aluminum silicate is a melt component. This approach yielded a melt with an aluminum saturation index (ASI = mol Al_2O_3/(mol alkali oxides + CaO + BaO)) of ~1.25, along with typically Mg-rich cordierite (e.g., Clemens and Wall 1988; Patiño Douce 1992; Icenhower 1995; see below).

Preparation of charges

Gold capsules (3×20 mm) were cleaned by soaking overnight in bromopropane (at 25 °C), and then by boiling for several hours in nitric acid. Afterwards, a few capsules still contained remnants of the extrusion lubricants used in the fabrication of the tubing, and these were removed with open-cell polyurethane foam swabs.

Low-impurity regions of gem-quality crystals were selected for crushing. Crystal fragments were microscopically hand sorted to remove impurities before grinding. Starting mixtures were ground in agate under ethanol to a mean grain size of 15 μm and dried in air at 110 °C. Powdered components were combined, ground together, dried (110 °C), and homogenized overnight in a tumbling mill. Water was loaded first, followed by powder mixes, into capsules (with additives confined to a central 5×3 mm portion of the capsule) which were sealed by arc welding. Capsules were checked for leaks after welding, and again after storage in a drying oven (110 °C). The heating step further allowed for homogenization of water (throughout powder) prior to experimental runs.

Equipment

Experiments were pressurized cold in Rene-41 and Nimonic-105 cold-seal reaction vessels using water plus trace Immunol as the pressure medium. Pressure was measured with a factory-calibrated Heise bourdon tube gauge. Fluctuations of < 3 MPa occurred over the course of experiments, with a total estimated accuracy of ± 10 MPa. Experiment duration varied from ~1 to 6 weeks. Temperature was monitored by internal vessel Chromel-Alumel thermocouples; estimated maximum

Table 1 Starting materials (added minerals)

Mineral[a]	Albite		Orthoclase		Quartz		Muscovite[b]		Biotite		Garnet-1		Garnet-2	
											$Alm_{44}Pyp_{42}Gro_{13}Sps_1$		$Alm_{46}Pyp_{44}Gro4Sps6$	
No. of analyses	5		20		6		1–3		96		20		20	
Oxide wt%														
SiO_2	68.82	(0.16)	64.95	(0.36)	99.99	(0.03)	51.91	–	38.83	(0.29)	39.71	(0.26)	39.53	(0.22)
TiO_2	n.d.		n.d.		n.d.		0.22	–	2.05	(0.11)	0.04	(0.02)	0.01	(0.01)
Al_2O_3	19.76	(0.05)	18.76	(0.14)	n.d.		28.02	–	11.26	(0.12)	23.20	(0.16)	23.14	(0.13)
Fe_2O_3	–		–		–		3.53	–	–		–		–	
FeO	n.d.		n.d.		n.d.		0.82[c]	–	18.47	(0.25)	21.26	(0.14)	22.05	(0.17)
MnO	n.d.		n.d.		n.d.		0.08	–	0.83	(0.04)	0.46	(0.02)	3.11	(0.09)
ZnO	n.d.		n.d.		n.d.		n.d.		0.14	(0.04)	n.d.		n.d.	
MgO	n.d.		n.d.		n.d.		1.00	–	14.08	(0.21)	11.46	(0.05)	11.89	(0.08)
CaO	0.07	(0.01)	0.01	(0.02)	n.d.		0.30	–	0.00	(0.01)	5.07	(0.04)	1.45	(0.02)
BaO	0.06	(0.05)	0.32	(0.04)	n.d.		0.09[d]	–	0.10	(0.02)	0.02	(0.02)	0.02	(0.02)
Na_2O	11.59	(0.04)	1.21	(0.07)	n.d.		1.27	–	0.56	(0.14)	0.00		0.00	
K_2O	0.23	(0.02)	14.84	(0.07)	n.d.		8.90	–	9.01	(0.14)	0.00		0.00	
Rb_2O (ppm)	n.d.		n.d.		n.d.		895[d]	–	n.d.		n.d.		n.d.	
Cs_2O (ppm)	n.d.		n.d.		n.d.		23[d]	–	n.d.		n.d.		n.d.	
P_2O_5	n.d.		n.d.		n.d.		n.d.		n.d.		0.04	(0.01)	0.07	(0.02)
F	n.d.		n.d.		n.d.		n.d.		3.67	(0.14)	0.02	(0.03)	0.01	(0.02)
Cl	n.d.		n.d.		n.d.		n.d.		0.05	(0.02)	0.01	(0.01)	0.00	
H_2O	n.d.		n.d.		n.d.		n.d.		2.02[d]	(0.08)	n.d.		n.d.	
LOI	–		–		–		3.87	–	–		–		–	
O = F									–1.54		–0.01		0.00	
O = Cl									–0.01		0.00		0.00	
Total	100.53	(0.18)	100.09	(0.40)	99.99	(0.03)	100.10	(0.16)[e]	99.52	(0.53)	101.28	(0.35)	101.28	(0.29)

[a]Albite, Copelinha, Minas Gerias, Brazil; orthoclase, St. Gotthard, Switzerland; quartz, ultrahigh purity, Feldspar Corp., Spruce Pine, NC, USA; muscovite, Spruce Pine, NC, USA; biotite, Ontario, Canada; garnet-1, Gore Mountain, NY, USA; garnet-2, laboratory standard

[b]Analyzed at Activation Laboratories Ltd. (Lancaster, Ontario, Canada) by X-ray fluorescence (fusion) unless otherwise specified

[c]Analyzed by titration

[d]Analyzed by instrumental neutron activation analysis. All other values are from quantitative electron probe microanalysis (with total iron as FeO). Numbers in parentheses represent 1 standard deviation of the mean. Propagated precision is shown for total values

[e]Estimated precision

error was ±5 °C. Experiments were quenched isochorically using compressed-air jet (5 to 15 °C/s). The fugacity of oxygen within capsules was not controlled, but regulated by diffusion of H_2 across the metal capsule walls. The fO_2 of the pressure medium is 0.5 log units below NNO (Huebner 1971) based on the measured solubility of cassiterite (Linnen et al. 1996). Following quench, capsules were weighed to check for leaks, punctured and the presence of free water was recorded. Capsules were then heated in a drying oven, and reweighed to verify loss of free water and hydration of glass (melt). All capsules gained minor weight during experiments by diffusion of Ni-metal (from vessels and filler rods) into the gold capsule walls, although none of the experimental products reported here, including biotite and cordierite, suffered detectable contamination by Ni.

Run pathways

Forward-direction experiments (prograde to run temperatures of 700 to 850 °C, designated as "F" in Table 2) promoted concurrent melting and new crystal growth. Reverse-direction experiments (designated as "R" in Table 3) were preconditioned by melting at 50 to 150 °C above the final T of the experiment, followed by isochoric quench to room temperature, and then run forward up to final temperatures in the range of 700 to 800 °C. These reverse-direction experiments induced crystal growth from melts that were substantially supersaturated in the crystalline phases at the final run T.

Analytical methods

Quantitative electron probe microanalysis (QEPMA)

All major- and minor-element oxide constituents of cordierite and glass products, except H, Li, Be, B, Rb and Cs, were analyzed using wavelength-dispersive spectroscopy on a Cameca SX-50 electron microprobe at the University of Oklahoma. Zinc and P were excluded from analyses of Crd because early analyses showed that their contents were at or below detection limits (≤ 0.05 or 0.02 wt% oxide, respectively). Analysis utilized crystalline and glass standards with TAP, PET, LIF, and a layered composite (PC1) diffraction devices. Operating conditions for hydrous glass analyses included a two-beam condition (2 nA and 20 nA regulated current) with a 20-μm spot size, in which Na and Al were analyzed first to inhibit beam-induced element migration effects (Morgan and London 1996). Analyses of minerals were conducted at 20 nA, 20 kV and a spot size of 3 to 5 μm. Counting times for all elements

Table 2 Cordierite–glass pairs from forward experiments

Run	BeP-56				BeP-60				BeP-57				BeP-58				BeP-68				BeP-105			
Mixture	SP-Crd-1				SP-Crd-1				SP-Crd-1				SP-Crd-1				SP-Crd-1				SP-Crd-2			
Final path/ duration (day)	700-F (26)				700-F (26)				750-F (26)				800-F (14)				800-F (17)				850-F (6)			
Crystalline products	Crd,Bt,Mag,Qtz,Pl				Crd,Bt,Mag,Qtz,Pl				Crd,Bt,Mag				Crd,Bt,Mag				Crd,Bt,Mag				Crd,Bt,Mag			
Analysis of	Crd		glass		Crd		glass		Crd		glass		Crd		glass		Crd		glass		Crd		glass	
No. analyses, QEPMA	7		11		20		10		10		11		10		11		16		10		10		12	
No. analyses, SIMS	2		2		2		3		2		2		2		2		2		3		1		1	
Wt%		SE		SD		SE		SD		SE		SD		SE		SD		SE		SD		SE		SD
SiO_2	46.47	(0.26)	70.95	(0.60)	48.42	(0.33)	70.83	(1.04)	48.25	(0.36)	70.57	(0.63)	48.25	(0.22)	70.01	(0.53)	48.27	(0.16)	70.79	(0.69)	49.14	(0.39)	69.23	(0.70)
TiO_2	0.02	(0.01)	0.05	(0.01)	0.01	(0.01)	0.01	(0.01)	0.01	(0.01)	0.02	(0.01)	0.02	(0.01)	0.12	(0.02)	0.01	(0.01)	0.09	(0.02)	0.01	(0.01)	0.10	(0.02)
B_2O_3 (ppm)	3	(0)	93	(2)	3	(1)	100	(1)	2	(0)	79	(0)	2	(0)	80	(0)	2	(0)	85	(1)	17	–	86	–
Al_2O_3	34.66	(0.18)	12.80	(0.25)	33.78	(0.14)	12.12	(0.18)	34.73	(0.16)	12.85	(0.12)	33.93	(0.13)	13.12	(0.25)	34.28	(0.11)	13.10	(0.12)	33.65	(0.29)	13.44	(0.18)
FeO	6.79	(0.17)	0.62	(0.05)	3.13	(0.09)	0.36	(0.03)	2.77	(0.09)	0.56	(0.05)	2.94	(0.02)	0.81	(0.05)	3.77	(0.08)	0.99	(0.17)	3.59	(0.20)	1.32	(0.07)
MnO	0.69	(0.04)	0.09	(0.01)	0.76	(0.03)	0.10	(0.01)	0.47	(0.02)	0.10	(0.02)	0.33	(0.02)	0.11	(0.01)	0.37	(0.02)	0.12	(0.01)	0.50	(0.03)	0.26	(0.02)
MgO	9.24	(0.16)	0.21	(0.01)	10.94	(0.11)	0.15	(0.02)	11.98	(0.07)	0.27	(0.01)	12.05	(0.05)	0.52	(0.01)	11.42	(0.07)	0.47	(0.01)	11.26	(0.21)	0.84	(0.02)
NiO	0.00		n.d.		0.01	(0.01)	n.d.		0.00		n.d.		0.00		n.d.		0.01	(0.01)	n.d.		0.01	(0.01)	n.d.	
ZnO	n.d.		n.d.		n.d.		n.d.		n.d.		n.d.		n.d.		n.d.		0.02	(0.02)	n.d.		0.02	(0.02)	n.d.	
BeO (ppm)	290.60	(16.21)	1.45	(0.07)	121.20	(19.41)	0.60	(0.05)	191.20	(11.20)	1.15	(0.03)	157.10	(9.80)	5.00	(0.20)	173.40	(16.29)	4.40	(0.56)	61.00	–	9.10	–
CaO	0.20	(0.03)	0.85	(0.04)	0.17	(0.01)	0.61	(0.09)	0.17	(0.01)	1.07	(0.07)	0.16	(0.02)	1.06	(0.09)	0.18	(0.02)	0.92	(0.08)	0.05	(0.01)	0.28	(0.06)
BaO	0.01	(0.01)	0.06	(0.03)	0.02	(0.02)	n.d.		0.01	(0.01)	0.05	(0.02)	0.02	(0.02)	0.05	(0.03)	n.d.		0.04	(0.03)	n.d.		0.07	(0.05)
Li_2O (ppm)	180	(22)	452	(9)	181	(12)	409	(8)	137	(1)	399	(7)	92	(12)	434	(3)	98	(2)	369	(18)	29	–	255	–
Na_2O	0.48	(0.05)	3.21	(0.10)	0.52	(0.04)	3.04	(0.11)	0.41	(0.06)	3.27	(0.10)	0.38	(0.02)	3.14	(0.12)	0.38	(0.01)	3.32	(0.13)	0.49	(0.03)	3.35	(0.08)
K_2O	0.06	(0.01)	3.31	(0.10)	0.10	(0.02)	3.61	(0.10)	0.08	(0.01)	3.37	(0.08)	0.12	(0.01)	3.36	(0.15)	0.11	(0.02)	3.19	(0.06)	0.32	(0.05)	3.49	(0.08)
Rb_2O (ppm)	5	(2)	104	(3)	8	(1)	134	(5)	7	(0)	110	(1)	8	(0)	110	(1)	8	(0)	102	(4)	23	–	119	–
Cs_2O (ppm)	2	(0)	9	(0)	2	(0)	11	(2)	2	(1)	14	(3)	4	(0)	12	(2)	5	(1)	7	(0)	4	–	7	–
	n.d.		0.12	(0.05)	n.d.		0.04	(0.03)	n.d.		0.11	(0.04)	n.d.		0.12	(0.03)	n.d.		0.06	(0.02)	n.d.		0.03	(0.03)
F	0.03	(0.03)	0.18	(0.04)	0.04	(0.04)	0.21	(0.05)	0.01	(0.01)	0.18	(0.07)	0.01	(0.01)	0.19	(0.07)	0.04	(0.03)	0.29	(0.09)	0.04	(0.04)	0.22	(0.07)
Cl	n.d.		0.01	(0.00)	0.00		0.00		n.d.		0.01	(0.01)	n.d.		0.01	(0.01)	0.00		0.01	(0.01)	n.d.		0.00	
O = F	–0.01		–0.08		–0.02		–0.09		0.00		–0.08		–0.01		–0.08		–0.02		–0.12		–0.02		–0.09	
O = Cl			0.00		0.00		0.00				0.00				0.00		0.00		0.00		0.00		0.00	
Total	98.69	(0.40)	92.43	(0.63)	97.91	(0.39)	91.03	(1.19)	98.92	(0.41)	92.39	(0.69)	98.22	(0.26)	92.58	(0.64)	98.85	(0.31)	93.31	(0.69)	99.05	(0.38)	92.57	(0.81)
H_2O by diff.	1.31		7.57		2.09		8.97		1.08		7.61		1.78		7.42		1.15		6.69		0.95		7.43	
ASI			1.21	(0.03)			1.20	(0.03)			1.16	(0.03)			1.21	(0.05)			1.23	(0.02)			1.36	(0.02)
Mg#	68.7	(1.7)			83.3	(2.4)			86.8	(2.8)			86.8	(0.6)			83.1	(1.8)			83.0	(4.6)		
D-B Crd/MELT	0.03	(0.00)			0.03	(0.01)			0.03	(0.00)			0.02	(0.00)			0.02	(0.00)			0.20			
D-Mn Crd/MELT	7.67	(0.96)			7.60	(0.82)			4.70	(0.96)			3.00	(0.33)			3.08	(0.31)			1.92	(0.19)		
D-Be Crd/MELT	200.41	(14.78)			202.00	(36.47)			166.26	(10.66)			31.42	(2.33)			39.41	(6.23)			6.70			
D-Ca Crd/MELT	0.24	(0.04)			0.28	(0.04)			0.16	(0.01)			0.15	(0.02)			0.20	(0.03)			0.18	(0.05)		
D-Li Crd/MELT	0.40	(0.05)			0.44	(0.03)			0.34	(0.01)			0.21	(0.03)			0.26	(0.01)			0.12			

D-Rb	0.05	(0.02)		0.06	(0.01)		0.06	(0.00)		0.07	(0.00)		0.08	(0.00)		0.20	
Crd/MELT																	
D-Cs	0.19	(0.00)		0.21	(0.04)		0.13	(0.08)		0.38	(0.06)		0.63	(0.14)		0.52	
Crd/MELT																	
Structural cations/18O																	
Si			4.77	(0.03)		4.92	(0.04)		4.85	(0.04)		4.88	(0.03)		4.87	(0.02)		4.94	(0.04)
Al			4.20	(0.03)		4.05	(0.02)		4.11	(0.03)		4.04	(0.02)		4.07	(0.02)		3.99	(0.04)
Be			0.01	(0.00)		0.00			0.00			0.00			0.00			0.00	
Total T sites			8.98	(0.04)		8.97	(0.05)		8.96	(0.05)		8.92	(0.03)		8.94	(0.03)		8.93	(0.06)
Li			0.01	(0.00)		0.01	(0.00)		0.01	(0.00)		0.00	(0.00)		0.00	(0.00)		0.00	(0.00)
Mg			1.42	(0.03)		1.66	(0.02)		1.79	(0.01)		1.82	(0.01)		1.72	(0.01)		1.69	(0.03)
Fe^{2+}			0.58	(0.01)		0.27	(0.01)		0.23	(0.01)		0.25	(0.00)		0.32	(0.01)		0.30	(0.02)
Mn			0.06	(0.00)		0.07	(0.00)		0.04	(0.00)		0.03	(0.00)		0.03	(0.00)		0.04	(0.00)
Total M site			2.07	(0.03)		2.01	(0.02)		2.07	(0.02)		2.10	(0.01)		2.07	(0.01)		2.03	(0.04)
Total			11.05	(0.05)		10.98	(0.05)		11.03	(0.05)		11.02	(0.03)		11.01	(0.03)		10.96	(0.07)
Channel occupants/18O																			
Ca			0.02	(0.00)		0.02	(0.00)		0.02	(0.00)		0.02	(0.00)		0.02	(0.00)		0.01	(0.00)
Na			0.10	(0.01)		0.10	(0.01)		0.08	(0.01)		0.07	(0.00)		0.07	(0.00)		0.10	(0.01)
K			0.01	(0.00)		0.01	(0.00)		0.01	(0.00)		0.02	(0.00)		0.01	(0.00)		0.04	(0.01)
H_2O			0.45	(0.00)		0.71	(0.00)		0.36	(0.00)		0.60	(0.00)		0.39	(0.00)		0.32	(0.00)
Total			0.58	(0.01)		0.84	(0.01)		0.47	(0.01)		0.71	(0.01)		0.49	(0.00)		0.47	(0.01)

1-Sigma precision is shown using standard error (SE) or standard deviation (SD) as appropriate

varied between 20 and 30 s. Data were reduced using PAP matrix correction routines (Pouchou and Pichoir 1985). Detection levels, taken at 3σ above mean background, were < 500 ppm for most elements. Similar experiments on Be-rich compositions indicate that Be is not lost to the capsule metal (Evensen and Meeker 1997).

Water contents of glass and cordierite were reported by difference methods from the combination of QEPMA and secondary ion mass spectrometry (SIMS). Hydrogen contents were measured by SIMS. But minor divergence in results compared to consistent convergence by QEPMA to established hydrous glass databases (Silver and Stolper 1989; Holtz et al. 1995, 1996) has been noticed in our laboratory (by QEPMA; A. Acosta and D. London 2002, unpublished data). Minor divergence was also noted between SIMS hydrogen contents and totals by QEPMA (cordierite), which led us to further favor the difference method over the range of compositions investigated here.

Images were acquired using both backscattered and secondary electron signals as 1,024×1,024 pixel data. Micrographs were processed (following Russ 1999) using either a low-pass or median filter (low-strength neighborhood ranking) for despeckling of noise. Images which contained minor periodic (instrumental) noise were corrected using Fourier transform processing techniques.

Secondary ion mass spectrometry

Samples were analyzed by SIMS using a Cameca Instruments IMS 3f at the Arizona State University at Tempe, AZ. A mass-filtered $^{16}O^-$ primary beam was accelerated through a potential of 12.5 kV, with a beam current of 1.0 nA. The focused spot size varied from 15 to 5 μm. Targets were mapped in advance and verified by imaging a combination of ^{7}Li, ^{9}Be, ^{23}Na, ^{26}Mg, ^{27}Al, ^{41}K, and ^{56}Fe before analysis.

Sputtered secondary ions were accelerated through a potential of 4.5 kV. The interference of $^{27}Al^{3+}$ (8.99384 a.m.u.) on ^{9}Be (9.01219 a.m.u.) is the most important concern in SIMS microanalysis of Be (Hervig 2002). The yield of ^{9}Be is substantially greater than the $^{27}Al^{3+}$ species when Be contents are high (e.g., Evensen 2001); the interference becomes negligible and no correction (voltage offset) is required. However, when Be contents are less than ~30 ppm, it has been observed (Grew et al. 1998) that trivalent Al begins to affect the analysis. Therefore, prior to and following each analysis, the mass collecting position was distinguished from $^{27}Al^{3+}$ and aligned to the ^{9}Be peak. Individual analyses consisted of collecting intensities on the following sequence of isotopes: ^{30}Si, ^{7}Li, ^{9}Be, ^{11}B, ^{85}Rb, ^{133}Cs, ^{30}Si. Integration times were sufficiently long to achieve a counting statistical precision of at least 3%. The count rates were normalized to that for Si and then to the silica abundance in the sample (derived from QEPMA).

A standard working curve for SIMS was calibrated for the analysis of Li, Be, B, Rb and Cs using glass standards and one crystalline standard. Three synthetic granitic glasses doped with Be (0.57, 1.11, or 3.33 wt% BeO by aqua regia ICP-AES, QEPMA, and SIMS; Evensen 1997) were used as standards for the analysis of experimental products. The glasses contained appreciable B, Li, Rb, and Cs (at concentrations far above those estimated for each element in unknowns), and therefore served as standards for the suite of elements in question. All trace elements were further calibrated against the NIST 610 glass, containing nominally ~500 ppm of the elements listed above (Pearce et al. 1997; Hinton 1999). Beryllian cordierite ("Sponda 454"; Armbruster and Irouschek 1983) was used to assess the convergence of ^{9}Be yields between crystalline and vitreous materials. These tests showed similar results to previous studies (e.g., Ottolini et al. 1993), with marked correlation between material responses along the working curve. Calibration factors derived from the standards listed above allowed the normalized count rates to be converted to absolute concentrations. Total internal and external precision (ICP) of BeO analyses of crystals and glass was $< 3.9\%$. Data were acquired in three sessions over a 2-year period. Between these sessions, the working calibration (Fig. 1) and SIMS results were highly reproducible (± 0.4 to 2.2%).

Table 3 Cordierite–glass pairs from reversed experiments

Run	BeP-95						BeP-96						BeP-19						BeP-97					
Mixture	SP-Crd-2						SP-Crd-2						SP-Crd-1						SP-Crd-2					
Prec. path/ duration (day)	850-F (6)						850-F (6)						850-F (6)						850-F (6)					
Final path/ duration (day)	700-R (34)						750-R (21)						800-R (16)						800-R (14)					
Crystalline products	Crd,Bt,Mag						Crd,Bt,Mag						Crd,Bt,Mag						Crd,Bt,Mag					
Analysis of	Crd				glass		Crd				glass		Crd				glass		Crd				glass	
	Cores		Rims				Cores		Rims				Cores		Rims				Cores		Rims			
No. analyses, QEPMA	8		14		10		11		12		12		10		6		10		11		17		12	
No. analyses, SIMS			1		2				2		5		1		1		2				1		3	
Wt%		SE		SE		SD		SE		SE		SD		SE		SE		SD		SE		SE		SD
SiO_2	49.01	(0.23)	49.04	(0.11)	72.03	(0.52)	47.88	(0.41)	47.96	(0.32)	70.89	(0.77)	48.54	(0.28)	49.73	(0.19)	70.51	(0.36)	47.49	(0.41)	49.10	(0.32)	71.39	(0.63)
TiO_2	0.01	(0.01)	0.01	(0.01)	0.03	(0.02)	0.01	(0.02)	0.01	(0.01)	0.05	(0.02)	0.02	(0.02)	0.02	(0.02)	0.08	(0.01)	0.02	(0.02)	0.01	(0.01)	0.10	(0.02)
B_2O_3 (ppm)	n.d.		7	–	124	(3)	n.d.		3	(0)	83	(4)	8	–	13	–	133	(10)	n.d.		10	–	98	(4)
Al_2O_3	33.21	(0.14)	33.54	(0.10)	12.05	(0.08)	33.79	(0.32)	33.18	(0.20)	12.24	(0.12)	33.63	(0.26)	32.88	(0.14)	12.97	(0.12)	34.39	(0.13)	34.18	(0.20)	12.65	(0.09)
FeO	4.78	(0.35)	3.86	(0.22)	0.39	(0.04)	5.72	(0.14)	8.03	(0.11)	0.78	(0.03)	2.68	(0.07)	2.46	(0.18)	0.75	(0.04)	5.02	(0.18)	2.88	(0.10)	0.61	(0.03)
MnO	0.98	(0.07)	1.21	(0.06)	0.16	(0.02)	0.83	(0.05)	1.06	(0.04)	0.20	(0.01)	0.27	(0.04)	0.34	(0.02)	0.10	(0.01)	0.70	(0.03)	0.72	(0.03)	0.20	(0.01)
MgO	9.73	(0.24)	10.25	(0.32)	0.17	(0.01)	9.41	(0.28)	8.45	(0.13)	0.21	(0.01)	12.74	(0.06)	12.38	(0.14)	0.45	(0.02)	10.28	(0.17)	11.58	(0.11)	0.38	(0.01)
NiO	0.01	(0.01)	0.01	(0.01)	n.d.		0.03	(0.01)	0.01	(0.01)	n.d.		0.01	(0.01)	0.01	(0.01)	n.d.		0.01	(0.00)	0.01	(0.01)	n.d.	
ZnO	0.02	(0.02)	0.02	(0.02)	n.d.		0.01	(0.01)	0.01	(0.01)	n.d.						n.d.		0.02	(0.02)	0.02	(0.02)	n.d.	
BeO (ppm)	n.d.		162.00	–	1.00	(0.18)	n.d.		195.80	(3.15)	1.40	(0.19)	16.00	–	201.00	–	6.55	(0.15)	n.d.		123.60	–	3.20	(0.29)
CaO	0.07	(0.02)	0.05	(0.01)	0.20	(0.05)	0.09	(0.02)	0.07	(0.02)	0.23	(0.06)	0.14	(0.02)	0.17	(0.02)	0.92	(0.06)	0.09	(0.06)	0.06	(0.02)	0.20	(0.05)
BaO	n.d.		n.d.		0.06	(0.03)	n.d.		n.d.		0.06	(0.04)	0.01	(0.01)	0.02	(0.02)	0.05	(0.03)	n.d.		n.d.		0.05	(0.03)
Li_2O (ppm)	n.d.		125	–	383	(5)	n.d.		80	(7)	267	(16)	56	–	56	–	444	(8)	n.d.		80	–	257	(16)
Na_2O	0.56	(0.04)	0.54	(0.09)	3.66	(0.13)	0.65	(0.06)	0.59	(0.05)	3.52	(0.08)	0.37	(0.05)	0.33	(0.03)	3.21	(0.10)	0.54	(0.06)	0.48	(0.03)	3.44	(0.09)
K_2O	0.15	(0.02)	0.12	(0.02)	3.64	(0.10)	0.35	(0.03)	0.16	(0.01)	3.41	(0.10)	0.12	(0.03)	0.22	(0.03)	3.33	(0.06)	0.18	(0.04)	0.20	(0.03)	3.73	(0.10)
Rb_2O (ppm)	n.d.		9	–	102	(0)	n.d.		12	(1)	111	(4)	10	–	11	–	127	(1)	n.d.		16	–	126	(4)
Cs_2O (ppm)	n.d.		3	–	11	(1)	n.d.		4	(0)	11	(0)	3	–	6	–	15	(0)	n.d.		2	–	7	(0)
P_2O_5	n.d.		n.d.		0.03	(0.02)	n.d.		n.d.		0.03	(0.02)	n.d.		n.d.		0.05	(0.02)	n.d.		n.d.		0.03	(0.02)
F	0.02	(0.02)	0.05	(0.05)	0.23	(0.06)	0.04	(0.04)	0.02	(0.02)	0.18	(0.05)	0.03	(0.03)	0.02	(0.03)	0.24	(0.09)	0.02	(0.03)	0.04	(0.04)	0.20	(0.05)
Cl	0.01	(0.01)	0		0.01	(0.00)	0		0		0.01	(0.01)	n.d.		n.d.		0.01	(0.00)	0		0.01	(0.01)	0.01	(0.00)
O = F	–0.01		–0.02		–0.10		–0.02		–0.01		–0.08		–0.01				–0.10		–0.01		–0.02		–0.08	
O = Cl					0.00		0		0		0.00						0.00		0		0.00		0.00	
Total	98.55	(0.38)	98.68	(0.43)	92.50	(0.67)	98.79	(0.61)	99.54	(0.42)	91.67	(0.84)	98.54	(0.40)	98.56	(0.33)	92.52	(0.44)	98.75	(0.50)	99.27	(0.41)	92.83	(0.68)
H_2O by diff.	1.45		1.32		7.50				0.46		8.33		1.46		1.44		7.48		1.25		0.73		7.17	
ASI					1.16	(0.03)					1.23	(0.03)					1.21	(0.02)					1.25	(0.03)
Mg#	75.0	(5.5)	78.2	(4.5)			71.9	(1.8)	62.3	(0.9)			88.5	(2.3)	88.7	(6.5)			76.2	(2.7)	85.1	(3.0)		
D-B Crd/ MELT			0.06						0.04	(0.00)					0.10						0.10			
D-Mn Crd/ MELT			7.56	(1.02)					5.30	(0.33)					3.40	(0.39)					3.60	(0.23)		
D-Be Crd/ MELT			162.00						139.86	(18.92)					30.69						38.63			

D-Ca Crd/		0.25	(0.08)				0.30	(0.12)				0.18	(0.02)				0.30	(0.13)		
MELT																				
D-Li Crd/		0.33					0.30	(0.03)				0.13					0.31			
MELT																				
D-Rb Crd/		0.09					0.11	(0.01)				0.09					0.13			
MELT																				
D-Cs Crd/		0.28					0.35	(0.00)				0.39					0.34			
MELT																				
Structural cations/18O																				
Si	4.99	(0.03)	4.96	(0.02)	4.89	(0.05)	4.90	(0.04)	4.89	(0.03)	5.00	(0.03)	4.84	(0.05)	4.92	(0.04)				
Al	3.98	(0.02)	4.00	(0.02)	4.07	(0.05)	4.07	(0.03)	3.99	(0.03)	3.89	(0.02)	4.13	(0.03)	4.03	(0.03)				
Be			0.00				0.00		0.00		0.00				0.00					
Total T sites	8.97	(0.04)	8.96	(0.03)	8.96	(0.07)	8.97	(0.05)	8.88	(0.05)	8.89	(0.03)	8.97	(0.06)	8.95	(0.05)				
Li			0.00				0.00		0.00		0.00				0.00					
Mg	1.48	(0.04)	1.55	(0.05)	1.43	(0.04)	1.44	(0.02)	1.91	(0.01)	1.85	(0.02)	1.56	(0.03)	1.73	(0.02)				
Fe^{2+}	0.41	(0.03)	0.33	(0.02)	0.49	(0.01)	0.47	(0.01)	0.23	(0.01)	0.21	(0.02)	0.43	(0.02)	0.24	(0.01)				
Mn	0.08	(0.01)	0.10	(0.00)	0.07	(0.00)	0.09	(0.00)	0.02	(0.00)	0.03	(0.00)	0.06	(0.00)	0.06	(0.00)				
Total M site	1.97	(0.05)	1.98	(0.05)	1.99	(0.05)	2.00	(0.02)	2.16	(0.01)	2.09	(0.03)	2.05	(0.03)	2.03	(0.02)				
Total	10.94	(0.06)	10.94	(0.06)	10.95	(0.08)	10.97	(0.05)	11.04	(0.05)	10.98	(0.04)	11.02	(0.06)	10.98	(0.05)				
Channel occupants/18O																				
Ca	0.01	(0.00)	0.01	(0.00)	0.01	(0.00)	0.01	(0.00)	0.02	(0.00)	0.02	(0.00)	0.01	(0.01)	0.01	(0.00)				
Na	0.11	(0.01)	0.11	(0.02)	0.13	(0.01)	0.12	(0.01)	0.07	(0.01)	0.06	(0.01)	0.11	(0.01)	0.09	(0.01)				
K	0.02	(0.00)	0.02	(0.00)	0.05	(0.00)	0.02	(0.00)	0.02	(0.01)	0.03	(0.00)	0.02	(0.00)	0.03	(0.00)				
H_2O			0.45	(0.00)			0.16	(0.00)			0.48	(0.00)			0.25	(0.00)				
Total	0.14	(0.01)	0.59	(0.02)	0.19	(0.01)	0.31	(0.01)	0.11	(0.01)	0.59	(0.01)	0.14	(0.01)	0.38	(0.01)				

Results

Experimental products

Synthesis of cordierite using Crd-free starting mixtures was successful for all compositions (Fig. 2a). Assemblages in forward-direction experiments (Table 2) contain cordierite + plagioclase + quartz + biotite + magnetite + melt (+ fluid) at 700 °C (Fig. 2b). In the 700 °C reversal, which was preconditioned at 850 °C, plagioclase and quartz are absent (Fig. 2c). We suggest that, at the preconditioning temperature, critical nuclei of plagioclase and quartz were probably removed (e.g., Lofgren 1983), thus inhibiting rapid nucleation at subliquidus temperatures (e.g., Marsh 1996). Plagioclase and quartz are lost by 750 °C, leaving the assemblage cordierite + biotite + magnetite + melt stable from 750 to 850 °C regardless of run direction (Fig. 2c–e).

Cordierite forms blocky euhedral crystals (5 to 150 μm in maximum section) in run products, sometimes containing minor inclusions of biotite or magnetite (Fig. 2b–e). In reversed experiments, the Mg:Fe ratio of cordierite reflects the temperature of growth (Table 3). Figure 2e, f shows reversed-direction cordierite products, in which the preconditioning step resulted in a more magnesian interior followed by an Fe-richer rim grown at lower T. Because of compositional zoning, crystal core and rim compositions were analyzed, but

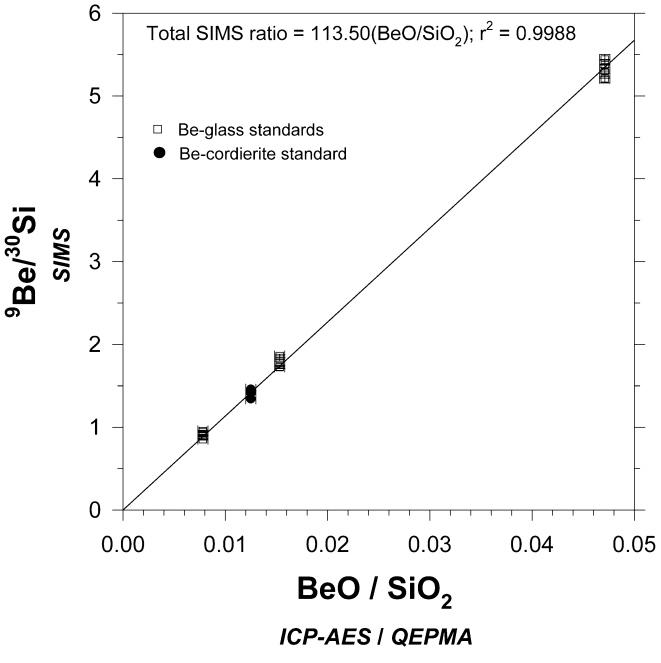

Fig. 1 Working curve for the analysis of beryllium by SIMS. Thirty-three data points are shown using standard glasses and natural beryllian cordierite analysed among three different sessions. The linear fit suggests no significant matrix effects for Be in rhyolitic glass and cordierite. Glass standards were previously characterized by aqua regia ICP-AES and QEPMA (Evensen 1997); cordierite was characterized by AA (“Sponda 454”; Armbruster and Irouschek 1983) and by QEPMA

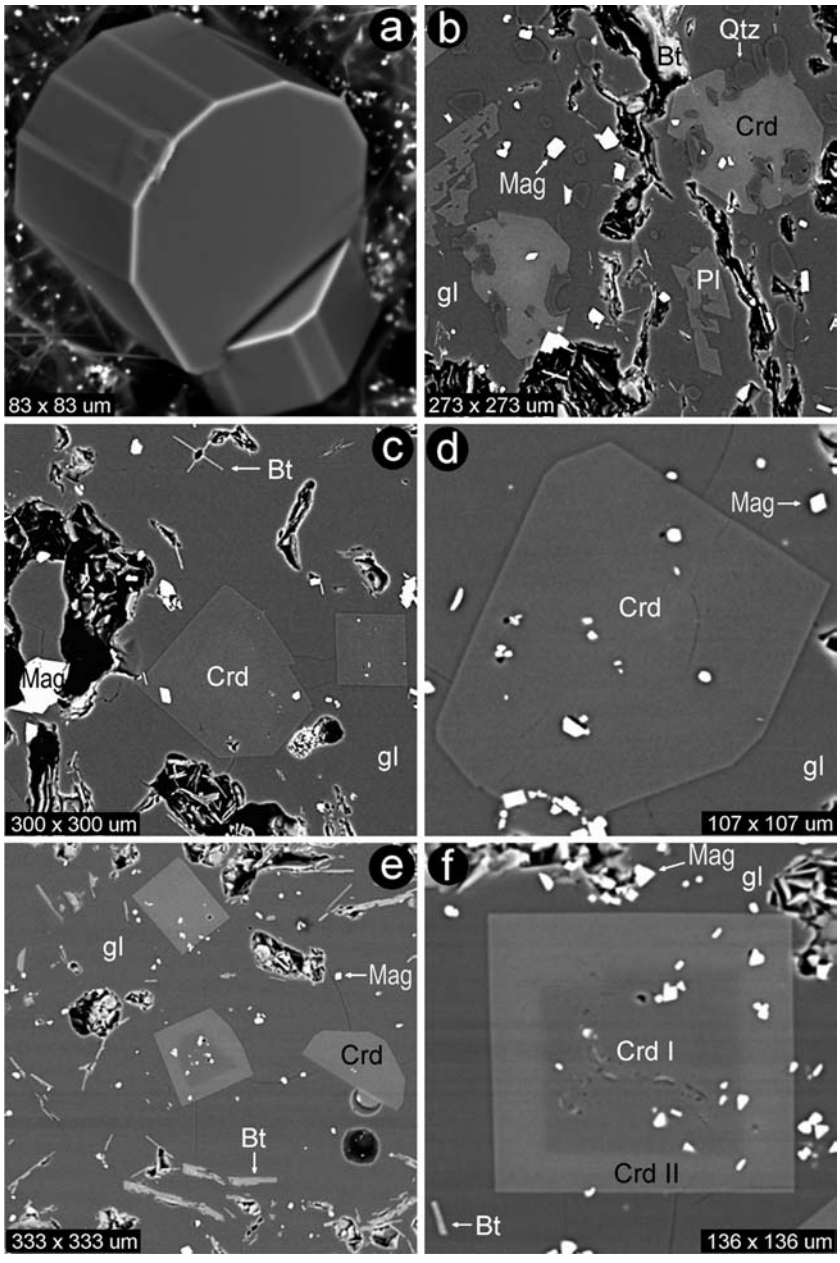

Fig. 2a–f Backscattered electron micrographs of experimental products and assemblages. Image scale is shown in micrometers. Phase abbreviations include *Crd* cordierite, *Bt* biotite, *Mag* magnetite, *Pl* plagioclase, *Qtz* quartz, and *gl* glass. **a** Cordierite crystals showing successful synthesis via Eq. (1). Needle-like white mica and magnetite are shown. **b** Forward experiment BeP-56: the assemblage contains Qtz and Pl in addition to Crd + Bt (also in vapor cavities) + Mag + melt + vapor. **c** Reversed experiment BeP-95: at temperatures ≥750 °C, the crystalline assemblage yields Crd + Mt + Bt in melt. Crystals of Crd and the glass pools represent typical targets amenable to analysis. **d** Forward experiment BeP-58: a characteristic, large Crd crystal is shown, stable with Mt, Bt (not shown), vapor and melt. **e** Reversed experiment BeP-62 (not analyzed for Be): early Mg-richer Crd cores (Mg# = 73.1) formed during the preconditioning step at 800 °C, whereas Fe-richer rims and new crystals of Crd (Mg# = 63.8) crystallized at the 750 °C lower T step. This pattern was commonly produced in reversed runs. **f** Magnified image in the same experiment as **d**, showing a high-T core of early-formed magnesian Crd (Crd I) with an intermediate Fe–Mg rim (Crd II) formed upon retrograde thermal conditions

only rim data were used for calculations of mineral/melt equilibria (see Evensen and London 2002). Plagioclase forms elongate and slightly skeletal crystals (20 to 80 μm) of albite–oligoclase. These crystals are commonly overgrown by a thick rim (5 to 15 μm) of andesine with skeletal character (Fig. 2b). Andesine also occurs as isolated crystals. Andesine forms in run products in which the starting composition contained the higher grossular component (garnet-1 in Table 1), suggesting the following reaction in the presence of melt:

$$\text{grossular} + Al_2SiO_5 + \text{quartz} = \text{anorthite}$$

Here, grossular makes up only a small component of garnet, aluminum silicate is a component of melt, and the anorthite component gives rise to andesine. We interpret albite–oligoclase growth to be a product of early-formed melt, whereas andesine crystallized later, commensurate with the complete dissolution of garnet. Such assemblages indicate the refractory nature of garnet relative to other crystalline phases.

Quartz mostly shows subhedral crystal morphology (3 to 30 μm), and is commonly poikilitically enclosed by cordierite. Biotite occurs both as elongated, compound crystal aggregates and as isolated crystals ranging in length from 10 to 100 μm, although some crystals may be as thin as 1 μm. Large, relict biotite crystals exhibit recrystallization, with new, fine-grained biotite + magnetite (equant crystals; 1 to 50 μm).

Cordierite and glass chemistry

Cordierite

Recalculated formulae and trace-element chemistry of Crd (Tables 2, 3) show changes with temperature. With increasing T from 700 to 850 °C, contents of the tetrahedral framework components SiO_2 and Al_2O_3 remain roughly constant. Over the same interval, BeO contents decrease from 291 to 61 ppm. Meanwhile, octahedral contents of Mg increase relative to Fe, and values of Mg# (=100×molar MgO/(MgO + FeO)) rise from 68.7 to ~85 over the interval above. Decreases are observed over the same conditions for concentrations of the other octahedral constituents, Mn (~1.21 to ~0.50 wt% MnO) and Li (180 to 29 ppm Li_2O).

Absolute amounts of channel-occupying components also vary over this range of T. Sodium contents remain roughly constant, decreasing only slightly with T. Potassium contents, however, rise steadily with T (from ~0.06 to ~0.32 wt% K_2O), and similar increases are seen for Rb and Cs (from 5 to 23 ppm Rb_2O, and from 2 to ~4 ppm Cs_2O). The large alkalis appear to be more easily accommodated with increasing T (e.g., Schreyer et al. 1990; Thompson et al. 2002) owing to structural expansion (e.g., Evans et al. 1980; Daniels 1992). Channel Ca and H_2O contents decrease with T (from ~0.20 to ~0.05 wt% CaO, and from 1.32 to ~0.73 wt% H_2O), but these data show scatter. Boron contents of cordierite are minor and also show scatter (from 3 to 22 ppm B_2O_3). Contents of Ti, Ni, Zn, Ba, P, F and Cl are at or below detection levels.

Mean values of recalculated cordierite formulae total 8.95 ± 0.01 and 10.99 ± 0.01 a.p.f.u. for total tetrahedral and octahedral cations, respectively (where ± values = standard error, std. error). These sums closely match the respective values of 9.0 and 11.0 which mark full occupancy. Total channel constituents (alkalis, Ca and H_2O) slightly decrease going from 700 to 850 °C (from ~0.84 to ~0.38 a.p.f.u.). Total channel occupancies show scatter from steady increases in K contents coupled with overall decreases in Na, Ca, and H_2O contents.

Peraluminous granitic melts

Silicic glasses in Tables 2 and 3 represent former melts in equilibrium with cordierite. These compositions contain normative components of corundum (Cor). Absolute contents of alumina in glass increase slightly going from 700 to 850 °C. The mean value of glasses on a normative haplogranite basis is $Ab_{31.11}Or_{22.56}Qz_{42.40}Cor_{3.93}$.

Elemental partitioning between cordierite and melt

Partition coefficients are shown in Tables 2 and 3 (following the notation of Beattie et al. 1993; $D_X^{min/melt} = X_{mineral}/X_{melt}$), and regression data for minor and trace elements as a function of temperature are shown in Table 4.

Of the nonessential elements in cordierite, only Be and Mn behave compatibly. Figure 3 shows that Be strongly partitions in favor of the cordierite structure with respect to peraluminous silicic melt. As T rises from 700 to 850 °C, $D_{Be}^{Crd/melt}$ values fall from 202.00 to 6.70 along a linear trend. The values illustrate the capacity of cordierite for sequestering Be in silicic melts, with extraordinary efficiency at lower temperatures. Values of $D_{Mn}^{Crd/melt}$ (Fig. 4) decrease linearly from 7.67 to 1.92 as T increases over the same range.

These experiments were conducted under conditions of water saturation, and the question arises regarding their applicability to hydrous but H_2O-undersaturated melts. The composition of the most beryllian cordierite composition known (Hölscher and Schreyer 1989; Evensen 2001), the saturating phase which closes the solvus crest ($Crd_{SS} + Brl_{SS}$) along the cordierite–beryl join in granitic melts (Evensen 2001; London and Evensen 2002), is approximately $(Mg,Fe)_2Al_2BeSi_6O_{18}\cdot 0.4H_2O$. With this H_2O content (cf. Harley and Carrington 2001; Harley et al. 2002), the activity product for this cordierite becomes

$$\underset{\text{Be-indialite(crystal)}}{[\alpha_{MgO}]^2[\alpha_{Al_2O_3}]^2[\alpha_{BeO}]^1[\alpha_{SiO_2}]^6[\alpha_{H_2O}]^{<1}} = \underset{\text{Be-indialite(melt)}}{[\alpha_{MgO}]^2[\alpha_{Al_2O_3}]^2[\alpha_{BeO}]^1[\alpha_{SiO_2}]^6[\alpha_{H_2O}]^{<1}} \quad (2)$$

It is clear that H_2O in channels exerts the least effect on the activity-composition relations, and that the incorporation of Be into Be-indialite hinges much more on the activities of silica, alumina, and Mg (also Fe, Mn) in melt. These relations suggest that the trend and magnitude of Be partitioning between cordierite and silicic melt at saturation in water will only be affected to a minor degree at water-undersaturated conditions.

Of the incompatible minor and trace elements (Fig. 4), distribution between Crd and melt occurs in the

Table 4 Regressions of elemental partitioning between cordierite and granitic melt as a function of temperature from 700 to 850 °C

D ratio	Linear fit	r^2 value
Compatible		
$D_{Be}^{Crd/MELT}$	D = 1,181.93–1.41(T)	0.9087
$D_{Mn}^{Crd/MELT}$	D = 35.46–0.04(T)	0.9712
Incompatible		
$*D_B^{Crd/MELT}$	$D = -0.42 + 6.38e^{-4}(T)$	0.3660
$D_{Li}^{Crd/MELT}$	$D = 1.61–1.733e^{-3}(T)$	0.7301
$*D_{Ca}^{Crd/MELT}$	$D = 0.60–4.88e^{-4}(T)$	0.2006
$D_{Rb}^{Crd/MELT}$	$D = -0.34 + 5.70e^{-4}(T)$	0.5015
$D_{Cs}^{Crd/MELT}$	$D = -1.28 + 2.12e^{-3}(T)$	0.5466

All values of temperature (T) are in °C.* T-independent

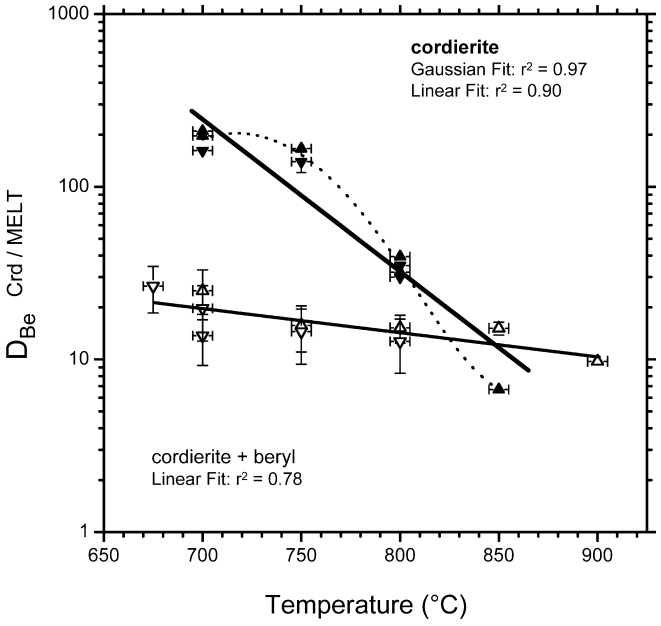

Fig. 3 Temperature-dependent partitioning of Be between cordierite and melt at 200 MPa. Ten data points are shown for cordierite formed in Be-poor melts (< 1s ppm Be in melt, this study); 12 data points are shown for beryllian cordierite formed at beryl saturation (10s to 100s ppm Be in melt, from Evensen 2001). *Upward-pointing triangles* designate forward experiments; *downward-pointing triangles* mark reverse experiments. *Error bars* signify 1σ propagated precision. A Gaussian distribution, D = (22,571/88.514×1.2533) exp –2((T–710)^2/7,834.7), best fits the cordierite data in the range of 700 to 850 °C but the linear trend, D = 8.6209–0.0089(T), should be used for extrapolation beyond these conditions. The linear fit of cordierite + beryl data is D = 2.2726–0.0014(T)

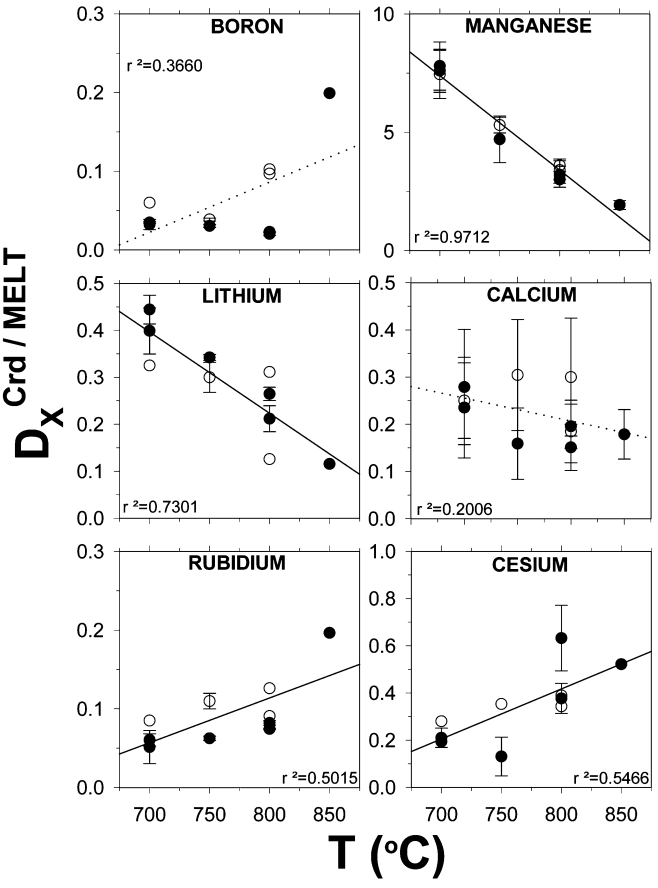

Fig. 4 Partition coefficients of selected elements between cordierite and melt at 200 MPa and at trace concentrations of these elements in melt. X-axes are constant but the scales of y-axes vary. Data from 10 experiments are displayed in each plot. Of the elements shown, only Mn is compatible. Partition coefficients of Mn and Li decrease with T, whereas those of Rb and Cs increase. Distributions of B and Ca do not vary significantly with temperature

following ways. Values of $D_{Li}^{Crd/melt}$, $D_{Rb}^{Crd/melt}$, and $D_{Cs}^{Crd/melt}$ decrease (from 0.44 to 0.12, 0.05 to 0.20, and 0.19 to ~0.60, respectively) as T rises from 700 to 850 °C. Partition coefficients for B show a slight increase (from 0.03 to ~0.13) with increasing T. Bimodal values of $D_{Ca}^{Crd/melt}$ (centered around 0.22 and 0.28) reflect a better correlation with starting composition than with run temperature. Boron and Ca distributions appear to be approximately independent of T, as low r^2 values suggest (Table 4).

Discussion

Experimental calibration of cordierite-associated trace elements of silicic melts

Beryllium

Beryllium mostly enters the cordierite structure by the exchange mechanisms $^{(4)}Be^{(ch)}(Na, K)^{(4)}Al_{-1}$ (low T) and $^{(4)}Be^{(4)}Si^{(4)}Al_{-2}$ (high T), which vary inversely with temperature (from 675 to 900 °C; Evensen 2001). Going from the trace levels of BeO in melt (this study) up to beryl saturation (Evensen et al. 1999), the measured $D_{Be}^{Crd/melt}$ values shift from 202.0 to 6.70 (from 700 to 850 °C) down to the narrower range of 26.6 to 15.1 (Fig. 3). With increasing contents of Be in melt, the mineral cordierite is saturating in Be, which leads to lower D-values. This classic behaviour of non-Henrian trace element distribution is influenced by increasing structural disorder, whereby the incorporation of significant contents of Be into cordierite results in hexogonal symmetry (e.g., Hölscher and Schreyer 1989; J.M. Evensen and D. London 2002, unpublished data). In peraluminous granitic melts, complete solid solution between cordierite and beryl exists.

In cordierite and beryl, Be resides in linking tetrahedra (e.g., Aurisicchio et al. 1988; Hölscher and Schreyer 1989), and shows a clear bond-angle preference (e.g., Downs and Gibbs 1981) for linking versus ring-forming geometries. Natural cordierite often contains moderate to very high contents of Be, generally ranging from 10s to 1,000s ppm. Cesium becomes more compatible in Be-rich Crd versus Be-poor Crd (Fig. 5), whereas Li and Mn behave similarly between Be-rich and Be-poor cordierite. Increasing $D_{Cs}^{Crd/melt}$ suggests that, in addition to increasing temperature (Daniels 1992), increased

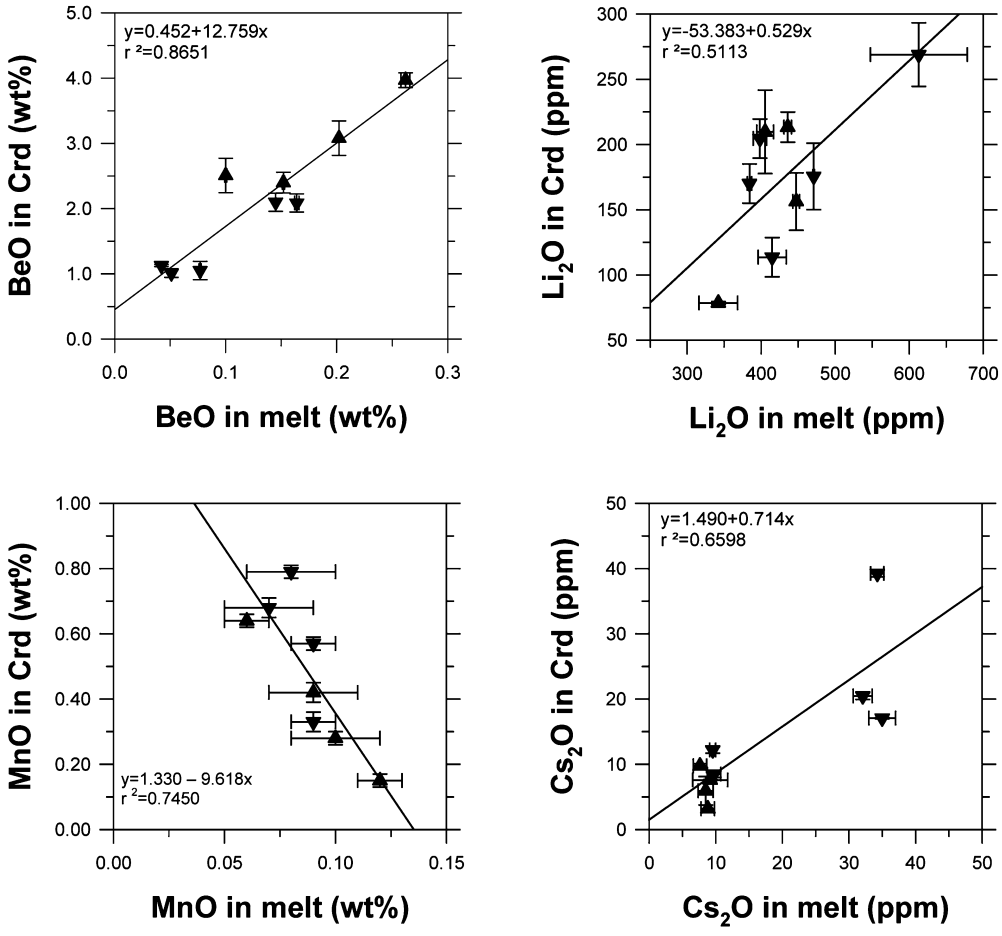

Fig. 5 Distribution of Li, Be, Mn, and Cs between cordierite and melt (200 MPa) at elevated melt activities of Li, Be and Cs (modified from Evensen 2001). All melts are saturated in beryl, and cordierite is appreciably beryllian (1.0 to 4.4 wt% BeO)

contents of Be may facilitate the widening of structural channel geometries.

White mica is commonly cited as the major source and control on Be contents of silicic rocks, originating from the relatively high contents of Be in marine sediment (e.g., 2 ppm; You et al. 1994) and pelite (e.g., 3 ppm; Turekian and Wedepohl 1961). In mica, Be replaces tetrahedral Al (brittle micas; $LiBeAl_{-1}$ or $HAlBe_{-1}$; Evensen and London 2002) or Si ($CaLiBeNa_{-1}Si_{-1}$; Grew et al. 1986), or a combination of these going from muscovite–paragonite to margarite-like structures. The result is an increase in tetrahedral ordering (e.g., Guggenheim 1984; Evensen et al. 2002) which structurally gives rise to the bityite end member ($CaLiAl_2BeAlSi_2O_{10}(OH)_2$). Polyhedral geometries of muscovite, however, are likely to be somewhat less accommodating for Be^{2+} compared to cordierite–beryl structures. In mica, Be contents typically range up to the 10s of ppm, and only rarely reach 100s of ppm (e.g., Wuensch and Hörmann 1978; Černý and Burt 1984; Grew et al. 1986; Smeds 1992). In experiments where the activity of beryllium in melt was varied, Be was found to be slightly compatible in muscovite ($D_{Be}^{Mus/melt} = 1.35$ at 700 °C, 200 MPa; Evensen and London 2002) at the lower Be concentrations applicable to the widest range of felsic magmas.

Compositions of cordierite and white mica, and their influence on whole-rock contents of Be, indicate that cordierite is far more effective in sequestering beryllium (Evensen and London 2002). Incorporation of Be into white mica becomes most important under cordierite-absent conditions. As a result, the budget of Be in melt is most susceptible to change when an S-type magma reaches the cordierite stability field.

Manganese

This transition metal gives rise to a distorted octahedral polyhedron which inhibits direct substitution into polyhedra that normally contain Fe^{2+} or Mg (e.g., Peacor and Wedepohl 1978; Burns et al. 1994). The partition coefficient for Mn between cordierite and peraluminous silicic melt is nearly identical to that of biotite melt at comparable P–T–X conditions. Values of $D_{Mn}^{Crd/melt}$ fall from 7.67 to 1.92 as T increases from 700 to 850 °C. Experimental values of $D_{Mn}^{Bt/melt}$ are reported to decrease from the range of 7.60 to 4.86 down to 3.78 to 3.50 as T rises from 650 to 750 °C (Icenhower and London 1995). Because the slopes of partition coefficients of Mn nearly overlap between cordierite/melt and biotite/melt, these minerals exert about the same

degree of control on the magmatic distribution of Mn. In the absence of garnet, which ultimately buffers Mn contents of melt (e.g., Icenhower et al. 1994; Icenhower 1995), it is the absolute abundance of Crd + Bt more than the relative ratio of these minerals that controls Mn in melt.

Lithium

Lithium enters the cordierite structure by substitution for octahedral R^{2+} cations, for example, by way of $Na^{(ch)}Li^{(6)}(Mg,Fe)^{(6)}_{-1}$ (Armbruster and Irouschek 1983; Kirchner et al. 1984; Gordillo et al. 1985; Černý et al. 1997; Evensen and London 2002). In the present experimental products, Li exhibits moderate to strong incompatibility in cordierite, depending on T ($D_{Li}^{Crd/melt} = 0.44$ to 0.12 going from 700 to 850 °C). Results support the usage of the difference in slope between Be and Li partition coefficients (i.e., values of Be/Li in Crd) as an indicator of T, so long as effects of melt/fluid activity of Be and Li are reconciled (see difference between slopes in Fig. 3). Cordierite exerts minor control on the Li contents of the melt. Lithium behaves compatibly in both white and dark micas (e.g., Icenhower and London 1995). Micas control the distribution of Li in melt.

Cesium

Cordierite accommodates Cs at channel sites. Figure 4 shows that Cs contents increase regularly with T, coincident with structural expansion and better accommodation for the large alkalis (e.g., Evans et al. 1980; Schreyer et al. 1990; Evensen 2001; Thompson et al. 2002). High-cordierite incorporates Cs by deformation of ring-forming tetrahedra in a manner which maintains symmetry (Daniels 1992). In cordierite–beryl solid solutions at 800 °C and higher, increasing Al/Si disorder and effects of distorted BeO_4 linking tetrahedra together widen channel sites to the extent that Cs becomes compatible (Evensen 2001).

At much higher contents of Cs_2O (~0.50 to 0.75 wt% versus ~several ppm Cs_2O in this study), Icenhower (1995) reported a mean value for $D_{Cs}^{Crd/melt}$ of 0.72 (±0.03) at 700 °C. This partition coefficient differs from the range of $D_{Cs}^{Crd/melt}$ in this study, which extends from ~0.19 to ~0.60 as T increases from 700 to 850 °C. At the low contents of Cs in most S-type magmas, uptake by cordierite is significant at 700 °C but much more efficient at higher T.

Cordierite-associated trace elements in granitic rocks

Cordierite-bearing granites

A survey of compositions which include complete light-element data (Table 5) illustrates that many S-type granites with Crd are distinguished by low Be concentrations in the whole-rock analysis (Evensen 2001; London and Evensen 2002). Compositions from more than 13 cordierite-bearing granites yield a mean of 0.80 ± 0.03 ppm Be. In comparison to granites worldwide, the Mn and Cs contents of the same rocks are noticeably low, showing mean values of 1.8 ppm Cs (range = 1.54 to 2.1) and 0.01 wt% MnO (range = 0.00 to 0.03).

In addition, cordierite-bearing granites do not seem to contain beryl in their pegmatitic differentiates (e.g., Barbey et al. 1999). Two trends emerge from the database: (1) an association between Crd-free granite and beryl-bearing pegmatite fields, or (2) an association between Crd-bearing granite (containing negligible Be in whole-rock values) and an absence of mineralized magmatic differentiates (e.g., Breaks and Moore 1993). Considering that Be is highly compatible in Crd, low Be contents of Crd-bearing granites require two more constraints – that their Crd is not restitic, but that restitic Crd was retained in the source regions. The validity of the second point follows from the negligible contribution of Crd to melting reactions at reasonable crustal temperatures (discussed below).

Cordierite-free granites

Compared to the above group, whole-rock values of these rocks are distinctly rich in Be, and may be associated with swarms of beryl-bearing pegmatites. Analyses of more than 100 cordierite-free granites, excluding their highly evolved facies (and mineralized products), yield a mean value of 6 ± 1.6 ppm Be (Evensen and London 2002). It is evident from the range of values reported in Table 5 that many such granites commonly contain even higher Be contents. Data in Table 5 also indicate a spatial correlation between these rocks, their beryl pegmatites and Be mineralization. About 115 analyses of the evolved facies of Crd-absent granites of S-type affinity yield a mean value of 69 ± 33 ppm Be with, once again, a range of values which usually extends even higher. Converted to BeO, this value equals ~400 ppm, which is near or beyond the melt saturation requirements for beryl in compositionally simple peraluminous haplogranitic melts at 700 °C (Evensen et al. 1999). However, Evensen et al. (1999) noted that beryl saturation is also a function of the other fluxing melt species, requiring higher BeO contents in B-, F-, and P-rich highly evolved melts. In summary, the database suggests that the Be contents of cordierite-free (mostly biotite ± garnet-bearing) peraluminous granitic magmas are up to 3 orders of magnitude higher than those of cordierite-bearing peraluminous granites.

Migmatites

Some of the most detailed data for evaluating the effect of Crd on magmatic signatures are contained in

migmatite analyses by Bea et al. (1994a), a subset of which is summarized in Table 6. Here, fractionation is evident between Crd-rich restite (melanosomes) and derived liquids (leucosomes). Relative to the Crd-bearing source rocks, the crystalline residua (restite) shows appreciable enrichments of Be, Mn and Cs. Physically separated leucogranite dikes, however, display marked depletions. Bea et al. (1994a) also estimated crystal/melt partition coefficients of migmatites using elemental contents of restitic minerals compared to those of genetically related leucosomes (melts). They noted preferential uptake of Be by Crd at a magnitude lower than most but within the range of $D_{Be}^{Crd/melt}$ experimental values reported here (near values similar to the higher T experiments, ~800 °C). They show Cs to be much more compatible in cordierite ($D_{Cs}^{Crd/leucosome} = 31.5$) than in our experimental results. Bea et al. (1994a) reported that Li was compatible in Crd as well, which is not supported by experimental studies to date (Icenhower and London 1995; this study).

Regional trace-element trends and pegmatite associations

Many S-type granitic rocks of western Europe contain cordierite in their assemblage, and some are interpreted to have originated by melting within the cordierite stability field (e.g., Bea et al. 1994a, 1994b). These granitic complexes or migmatite fields are conspicuously devoid of Be enrichment except for the few analyses of their restitic counterparts (e.g., melanosomes with 3.51–8.10 ppm Be, see Table 5) or cordierite-rich cockades (3.4–7.1 ppm Be; Barbey et al. 1999). Using the partitioning data for Be, this trend logically suggests that the low range of Be in such granites can be accounted for by the retention of Be in restitic Crd, followed by restite unmixing.

Of the few reported Be contents of granites, those of Portugal (Charoy and Noronha 1996; Ramirez and Grundvig 2000) are distinctly higher than the nearby peraluminous granites of Spain (e.g., Bea et al. 1994b). Even in studies in which Be was not analyzed, Cs and Mn contents of granites in central Portugal are notably greater than in Crd-bearing granites (e.g., Neiva et al. 1987). This contrast likely indicates magma formation at the generally low pressures of cordierite stability for many granite provinces of Spain, but deeper, higher-temperature sources for granites of Portugal – in the field of garnet + Al_2SiO_5. In North America, beryl-bearing pegmatites are common – suggesting generally deeper, higher-temperature sources of granitic magmatism. These systems are often associated with Crd-free, S-type granites of the inner Cordillera (e.g., Miller and Bradfish 1980) and continental interior (e.g., garnet-bearing Harney Peak granite, South Dakota; e.g., Shearer et al. 1987; Norton and Redden 1990; garnet- and orthopyroxene-bearing granites associated with the Treelined Lake complex, Ontario; e.g., Pan and Breaks 1997).

Based on the high compatibility of Be in cordierite, we expect that restitic Crd becomes increasingly rich in Be with the progress of prograde reactions, e.g., Crd = Be–Crd + melt. This tendency explains the occurrence of *cordieritites*, comprised dominantly of Crd-rich restite, where the Be contents of Crd reach 1 wt% BeO (Schreyer et al. 1979). The decomposition of Be-enriched cordierite can be a source of Be for other phases. For example, Grew (1998) and Baba et al. (2000) propose that the breakdown of Be-rich cordierite provided the source of Be for surinamite-bearing pegmatites in Antarctica. This is in contrast to the generally low contents of Be in most metamorphic rocks (Grew 2002).

The normative cordierite component of peraluminous melt

Where Crd makes up a large portion of the mode of a rock (e.g., ~60 to 90%), it is commonly interpreted as being restitic in origin (residual crystals or produced by reaction with wall rock; Gordillo 1979; Ugidos 1988, 1990; Kamber et al. 1998; Kalt et al. 1999), although it has been debated whether Crd was restitic or precipitated directly from melt (e.g., Ugidos and Recio 1993). We have already provided one means of making this distinction: the Be content of Crd which has precipitated from restite-free melt will be much lower than in Crd of the restite. Using this measure, then the low Be contents of Crd-bearing leucogranites of western Europe (Table 5) signify that the Crd in those granites is magmatic, not restitic. The compositions of experimental glasses produced here (Tables 2 and 3) provide another constraint. As these glasses represent melts which are saturated in Crd, we can calculate a normative Crd component of those glasses to estimate how much Crd could crystallize from them. The calculations are drawn from the glass composition at 700 °C from Tables 2 and 3, which represents the composition in this study nearest to the granite minimum.

Normative Crd contents of this glass are displayed in Table 7. Depending on the choice of phases present, the normative Crd component is limited either by Al or by Mg(Fe). Magnesium and Fe are distributed between coexisting micas, magnetite, and cordierite using recalculated formulae for these minerals from experiments. The products show that the normative component of cordierite in peraluminous granitic melt varies from 0 to a maximum of 4.0% as the muscovite content varies antipathetically from about 5 to 0%. For cases corresponding to Crd-producing reactions, such as Bt + Sil (2nd) = Crd + L, a maximum of 4% Crd is generated in the norm. When other peraluminous crystalline phases are present with Crd, a common condition of natural rocks, normative values of less than 4% Crd result. Many Crd-bearing granites are frequently Mus-poor, which corresponds to a higher values of Crd (~3%). Most Crd-bearing granites, however, are relatively Bt-rich. After the Al component of the calculation, Mg

Table 5 Reported Be contents of granitic rocks and their association to cordierite-bearing source rocks

Granitic sample	Crd-bearing rock	Beryl-bearing pegmatites?	Be (ppm)			Cs (ppm)			MnO (wt%)			*n*	Granite body	Location	Reference
			Mean	SE	Range	Mean	SE	Range	Mean	SE	Range				
Leucosome	Restite, leucosome		1.20	0.10	0.37–2.04	1.54	0.06	0.93–2.01	0.02	0.00	0.01–0.02	6	Pena Negra Complex	Central Spain	Bea et al. (1994a)
Main granite	Restite, leucosome, granite		0.4	–	–	–	–	–	0.00	–	–	1	Antragigues leucogranite	Massif Central, France	Barbey et al. (1999)
Main granite	Restite, leucosome, granite		1.1	–	–	–	–	–	0.03	–	–	1	Le Roux granite	Massif Central, France	Barbey et al. (1999)
Main granite	Granite		< 1	–	–	2.1	0.21	1.7–2.8	0.01	0.00	0.00–0.01	5	Ghost Lake batholith	Ontario, Canada	Breaks and Moore (1993)
Upper granite	No Crd	Brl pegmatites	3	1	2–4	7.7	–	–	0.02	0.00	–	2	Ghost Lake batholith	Ontario, Canada	Breaks and Moore (1993)
Upper facies	No Crd		4.3	0.3	3.7–4.5	23.5	4.7	17.7–32.8	0.02	0.01	0.01–0.03	11	Pedroberardo pluton	Central Spain	Bea et al. (1994b)
Middle facies	No Crd		4.0	0.2	3.5–4.4	9.9	0.5	8.8–11.1	0.03	0.00	0.02–0.03	12	Pedroberardo pluton	Central Spain	Bea et al. (1994b)
Lower facies	No Crd		4.1	0.5	2.9–4.8	9.7	1.2	6.7–12.5	0.02	0.00	–	14	Pedroberardo pluton	Central Spain	Bea et al. (1994b)
Central granite	No Crd	Brl pegmatites	4.0	0.3	3.6–4.3	11.0	3.1	7.9–14	0.07	0.00	0.06–0.07	2	Port Mouton pluton	S. Nova Scotia, Canada	Currie et al. (1998)
Central granite	No Crd	Brl pegmatites	4.1	0.3	3.0–5.1	6.1	1.0	4.2–8.8	0.05	0.01	0.02–0.07	4	Shelburne pluton	S. Nova Scotia, Canada	Currie et al. (1998)
Granite facies	No Crd	Brl pegmatites	5	1	4–7	–	–	–	0.02	0.00	0.02–0.03	32	Sparrow granite	NWT, Canada	Kretz et al. (1989)
Central granite	No Crd		12	1	4–33	40	3	9.1–81.5	0.039	0.001	0.024–0.074	10	Tin-rich granites	NW Bohemia	Breiter et al. (1991)
Main granite	No Crd	Brl pegmatites	8	–	–	–	–	–	–	–	–		Harney Peak granite	South Dakota, USA	Norton and Redden (1990)
Upper facies	No Crd	Brl pegmatites	11.4[a]	–	5.7–17	32[a]	–	14–50	0.09[a]	–	0.03–0.14		Elkhorn, Harney Peak granite	South Dakota, USA	Shearer et al. (1987)
Evolved facies	No Crd	Brl pegmatites	64.0[a]	–	28.0–100	17[a]	–	10–23	0.14[a]	–	0.05–0.22		Sky Lode, Harney Peak granite	South Dakota, USA	Shearer et al. (1987)
Major facies	No Crd		6.1	0.3	3.8–8.0	23.5	1.1	11.1–45.2	0.61	0.03	0.19–0.99	10	Jalmala pluton	Central Spain	Ramirez and Grundvig (2000)
Evolved facies	No Crd		11.0	3.0	8.0–16.95	44.2	2.5	39.4–53.0	0.21	0.01	0.18–0.25	3	Jalmala pluton	Central Spain	Ramirez and Grundvig (2000)
Apical granite	No Crd	Brl pegmatites	11	2	9–12	14	2	12–15	0.05	0.00	0.05–0.06	3	Leinster granite	SE Ireland	Luecke (1981), Kennan (2001)
Evolved facies	No Crd	Brl pegmatites	11	5	6–25	47	33	13–145	0.06	0.01	0.06–0.10	4	Leinster granite	SE Ireland	Luecke (1981), Kennan (2001)
Evolved microgranite	No Crd	Accessory Brl	130	31	34–385	224	14	60–350	0.05	0.00	0.04–0.06	10	Argemela granite	Central Portugal	Charoy and Noronha (1996)
Evolved facies	No Crd	Be-phosphates	123	13.2	5.7–494	305	38.1	32.5–1471	0.044	0.003	0.014–0.106	95	Beauvoir granite	Massif Central, France	Raimbault et al. (1995)
Average Be content of granite with early Crd			0.9	0.3	0.4–1.20	1.54	–	–	0.02	0.01	0.00–0.03				

Average Be content of granite with late Crd	0.7	0.2	< 1–1.1	2.1	–	–	0.01	0.01	0.00–0.03
Average Be content of Crd-bearing granite (at any stage)	0.8	0.2	< 1–1.20	1.8	0.3	1.54–2.1	0.01	0.01	0.00–0.03
Average Be content of Crd-free main granite	6	1.7	3–12	18	3.6	6.1–40	0.09	0.05	0.02–0.61
Average Be content of granite with associated Brl pegmatites	14	8.4	3–64	15	4.7	6.1–32	0.06	0.02	0.02–0.14
Average Be content of evolved granite facies	68	25.9	11–130	127	58	17–224	0.10	0.03	0.05–0.21

[a]Median values

becomes limiting. Thereby, a Bt-rich assemblage yields a normative Crd component closer to the lower end (~0%). Table 7 shows that with 5 norm% Bt, the normative Crd component falls to 0.25% (with a remainder allotted to corundum). In short, the most reasonable value is variable but intermediate between 0 to 4 norm% Crd. When Crd constitutes more than a few percent of a natural mode, the assemblage in question could not have originated strictly by condensation from melt, although Crd and other restitic phases may recrystallize in the presence of (i.e., via) the melt phase (e.g., Icenhower and London 1995). This conclusion reinforces our prior statements: most of the Be in the protoliths for an S-type magma will be retained in restitic Crd, as only a small fraction of Crd component is actually contributed to the melt.

Conclusions

Cordierite and the S-type granite signature

White et al. (1986a) and Zen (1987) suggested using cordierite as an indicator of S-type granitic source terranes. Although most phase equilibrium investigations have stressed the importance of cordierite for the generation of S-type silicic melts (e.g., Green 1976; Clemens and Wall 1981; Vielzeuf and Holloway 1988; Patiño Douce 1992; Fitzsimons 1994), cordierite actually constitutes a minor to negligible component of melts, even those which remain Crd-saturated. We suggest that the importance of cordierite may lie mostly in its impact on the trace-element signatures of S-type magmas.

The results of this study suggest that cordierite, more than any other rock-forming mineral, controls the distribution of magmatic Be and Cs. Lithium budgets of melts are controlled by micas, and biotite and cordierite both affect the distribution of Mn. The ranges of mean values of 0.8 versus 6 ppm Be (Table 5) clearly separate populations of Crd-bearing from Crd-free granites. The only slight overlap is seen for MnO contents, which again reflects a dual control on its distribution by Crd and Bt. In decreasing order of the efficiency of accommodation by cordierite, the cordierite-associated, S-type trace-element signature is comprised of:

Be – Cs – Mn – Li

If cordierite is part of the anatectic assemblage during melting, the greater the degree for residual crystals to equilibrate with derived liquid, the more this suite of elements will be lost by incorporation into cordierite. Granites originating within the stability field of cordierite will carry low Be signatures, whereas magmas which originate within the mid-crustal (and deeper) garnet + Al_2SiO_5 stability field may achieve cordierite saturation by shallow-level crystallization (e.g., Barbey et al. 1999) or igneous fractionation (e.g., from Opx- to

Table 6 Reported Be contents of migmatite systems: Pena Negra Complex, central Spain (Bea et al. 1994a)

Migmatite facies	Crd-bearing?	Be (ppm)			Cs (ppm)			MnO (wt%)			*n*
		Mean	SE	Range	Mean	SE	Range	Mean	SE	Range	
Mesosome	Yes	2.34	0.65	1.13–4.75	5.69	0.35	4.89–6.58	0.07	0.01	0.05–0.11	5
Melansome	Yes	6.04	1.35	3.51–8.10	13.47	1.04	11.6–15.2	0.13	0.01	0.10–0.15	3
Leucosome	Yes	1.20	0.10	0.37–2.04	1.54	0.06	0.93–2.01	0.02	0.00	0.01–0.02	6

Table 7 Cordierite-bearing normative calculations of melt at 700 °C

Input conditions for iteration[a]	Limiting Crd component	Norm							
		Ab	Or	Qtz	Cor	Mus	Bt	Mt	Crd
0% Cor, Bt, Mus	Al	17.5	13.7	64.6	0	0	0	0.3	4.0
5% Bt	Mg	19.1	12.1	60.6	2.3	0	4.9	0.7	0.3
5% Mus	Mg	17.5	9.9	65.0	1.0	4.8	0.6	0.2	1.0
8% Mus	Mg	17.5	7.4	65.0	0	8.4	0.5	0.3	1.0
10% Mus	Al	17.5	6.2	65.4	0	9.6	1.0	0.2	0.1

[a]Following the initial conditions, the remainder of the mode was calculated by allocating moles of Mg equally between Bt and Crd using the stoichiometry of their recalculated formulae (Tables 2, 3)

Crd-bearing assemblages; Secchi et al. 1991), and may thus contain significantly higher Be contents. Moving from regional to local scales, Be signatures track reaction between granite magmas and Crd-bearing versus Crd-free country rocks, where strong fluctuations in Be and other trace-element contents may locally be manifested (e.g., Kretz et al. 1989) as a function of proximity to Crd-bearing rock.

Where anatexis of a metasedimentary protolith occurs beyond the relatively low-pressure environment of cordierite stability, the suite of elements above will fractionate into the melt, their budgets thereafter being controlled mainly by white (Li, Be, Cs) and dark (Li, Mn, F) micas. Other essential contributors to the F, P, and B signatures in S-type systems are dark mica (sensu lato, including biotite and Li-bearing dark mica; Icenhower and London 1995; London 1995), apatite and other phosphates (Watson and Capiobianco 1981; Wolf and London 1994; London et al. 1999), and tourmaline (e.g., Wolf and London 1997), respectively. For a single mineral, however, the breadth of elements incorporated by cordierite is extensive. Surveys of whole-rock compositions, in addition to association with or without beryl-bearing pegmatites, indicate that a major fraction of granite bodies contained cordierite in their residua.

Clearly, cordierite imparts or, more often, removes an S-type trace-element signature from granitic melts. Cordierite-bearing and cordierite-free peraluminous granites are separated by about an order of magnitude in concentrations of Be, Cs and Mn. Unlike micas, the cordierite signature resolves the source of melting within relatively narrow stability field limits. Routine analysis of Crd, and Be, in conjunction with established $D_{Be,Cs,Mn}^{Crd/melt}$ relations, offer means to discriminate residual versus magmatic mineralogy – an issue central to the interpretation of S-type granites (e.g., White et al. 1986a, 1986b; Ugidos and Recio 1993). In the end, the unique capacity of the cordierite crystal structure to accommodate a diverse range of ions, from those requiring the smallest (Be) to the largest (Cs) coordination polyhedra, largely controls the magmatic budgets of these petrologically and economically important lithophile trace elements.

Acknowledgements This work was supported by National Science Foundation EAR-9625517, 9618867, and 990165, and by the Society of Economic Geologists Foundation and the American Association of Petroleum Geologists Grants-in-Aid Program. The Electron Microprobe Laboratory was created by Department of Energy grant DE-FG22–87FE1146 with assistance from NSF GIF EAR-9404658 and support from the University of Oklahoma. We gratefully acknowledge Richard Hervig (Arizona State University) for helping with the interpretation of SIMS results, and George Morgan (University of Oklahoma) for helping with the interpretation of QEPMA results. We thank Thomas Armbruster (University of Bern) for donating beryllian cordierite from Alpe Sponda for calibration of our SIMS working curve. We appreciate helpful discussions with Antonio Acosta (University of Oklahoma), and thoughtful reviews by Simon Harley (University of Edinburgh) and John Clemens (Kingston University) which improved the manuscript.

References

Armbruster T, Irouschek A (1983) Cordierites from the Lepontine Alps: Na + Be→Al substitution, gas content, cell parameters, and optics. Contrib Mineral Petrol 82:389–396

Aurisicchio C, Fioravanti G, Grubessi O, Zanazzi PF (1988) Reappraisal of the crystal chemistry of beryl. Am Mineral 73:826–837

Baba S, Grew ES, Shearer CK, Sheraton JW (2000) Surinamite, a high-temperature metamorphic beryllosilicate from Lewisan sapphirine-bearing kyanite- orthopyroxene-quartz potassium feldspar gneiss at South Harris, N.W. Scotland. Am Mineral 85:1474–1484

Barbey P, Marignac C, Montel JM, Macaudiere J, Gasquet D, Jabbori J (1999) Cordierite growth textures and the conditions of genesis and emplacement of crustal granitic magmas; the Velay granite complex (Massif Central, France). J Petrol 40:1425–1441

Bea F (1996) Controls on the trace-element composition of crustal melts. Trans R Soc Edinb 87:33–41

Bea F, Pereira MD, Stroh A (1994a) Mineral/leucosome trace-element partitioning in a peraluminous migmatite (a laser ablation-ICP-MS study). Chem Geol 117:291–312

Bea F, Pereira MD, Corretge LG, Fershtater GB (1994b) Differentiation of strongly peraluminous, perphosphorus granites: the Pedrobernardo pluton, central Spain. Geochim Cosmochim Acta 58:2609–2627

Beattie P, Drake M, Jones J, Leeman W, Longhi J, McKay G, Nielsen R, Herbert P, Shaw D, Takahashi E, Watson B (1993) Terminology for trace element partitioning. Geochim Cosmochim Acta 57:1605–1606

Breaks FW, Moore JM Jr (1993) The Ghost Lake batholith, Superior Province of northwestern Ontario: a fertile S-type, peraluminous granite – rare-element pegmatite system. Can Mineral 30:835–875

Breiter K, Sokolova M, Sokol A (1991) Geochemical specialization of the tin-bearing massifs of NW Bohemia. Miner Deposita 26:298–306

Burns PC, MacDonald DJ, Hawthorne FC (1994) The crystal chemistry of manganese-bearing elbaite. Can Mineral 32:31–41

Carrington DP, Harley SL (1995) Distribution of water between cordierite and granitic melts determined by SIMS. Terra Abstr 7(1):297

Černý P, Burt DM (1984) Paragenesis, crystallochemical characteristics, and geochemical evolution of micas in granite pegmatites. In: Bailey SW (ed) Micas. Mineral Soc Am Rev Mineral 13:257–298

Černý P, Chapman R, Schreyer W, Ottolini L, Bottazzi P, McCammon CA (1997) Lithium in sekaninaite from the type locality, Dolní Bory, Czech Republic. Can Mineral 35:167–173

Chappell BW (1999) Aluminum saturation in I- and S-type granites and the characterization of fractionated haplogranites. Lithos 46:535–551

Chappell BW, White AJR (1974) Two contrasting granite types. Pacific Geol 8:173–174

Charoy B, Noronha F (1996) Multistage growth of a rare-element, volatile-rich microgranite at Argemela (Portugal). J Petrol 37:73–94

Clemens JD, Wall VJ (1981) Origin and crystallization of some peraluminous (S-type) granitic magmas. Can Mineral 19:111–131

Clemens JD, Wall VJ (1988) Controls on the mineralogy of S-type volcanic and plutonic rocks. Lithos 21:53–66

Currie KL, Whalen JB, Davis WJ, Longstaffe FJ, Cousens BL (1998) Geochemical evolution of peraluminous plutons in southern Nova Scotia, Canada – a pegmatite-poor suite. Lithos 44:117–140

Daniels P (1992) Structural effects of the incorporation of large-radius alkalis in high cordierite. Am Mineral 77:407–411

Downs JW, Gibbs GV (1981) The role of the BeOSi bond in the structures of beryllosilicate minerals. Am Mineral 66:819–826

Evans DL, Fisher GR, Geiger JE, Martin FW (1980) Thermal expansions and chemical modifications of cordierite. J Am Ceram Soc 63:629–634

Evensen JM (1997) Effects of beryllium on the liquidus phase relations of haplogranite. MSc Thesis, Colorado School of Mines, Golden, Colorado

Evensen JM (2001) The geochemical budget of beryllium in silicic melts, and superliquidus, subliquidus, and starting state effects on the kinetics of crystallization in hydrous haplogranite melts. PhD Dissertation, University of Oklahoma, Norman

Evensen JM, London D (2002) Experimental silicate mineral/melt partition coefficients for beryllium and the crustal Be cycle from migmatite to pegmatite. Geochim Cosmochim Acta 66:2239–2265

Evensen JM, Meeker GP (1997) Feasibility of Be analysis for geologic materials using EPMA. In: Proc Microscopy and Microanalysis 1997. Microscopy Society of America, vol 3(2), pp 893–894

Evensen JM, London D, Wendlandt RF (1999) Solubility and stability of beryl in granitic melts. Am Mineral 84:733–745

Evensen JM, London D, Hughes JM, Rakovan JF, Hervig RL, Kaszuba JP (2002) Crystal chemistry, crystallography and petrogenesis of the beryllium micas. Int Mineral Assoc Programme Abstr 18:MH12, 207

Fitzsimons ICW (1994) Cordierite migmatites from East Antarctica; geochemical constraints on volatile distribution during crustal anatexis. Mineral Mag 58A:274–275

Gordillo CE (1979) Obervacionnes sobre la petrología de las rocas cordieríticas de la Sierra de Córdoba. Bol. Acad Nac Cienc Cordoba Argentina 53:3–44

Gordillo CE, Schreyer W, Werding G, Abraham K (1985) Lithium in NaBe-cordierites from El Peñón, Sierrra de Córdoba, Argentina. Contrib Mineral Petrol 90:93–101

Green TH (1976) Experimental generation of cordierite- or garnet-bearing granitic liquids from a pelitic composition. Geology 4:85–88

Grew ES (1998) Boron and beryllium minerals in granulite-facies pegmatites and implications of beryllium pegmatites for the origin and evolution of the Archean Napier Complex of East Antarctica. Mem Natl Inst Polar Res Spec Issue 53:74–92

Grew ES (2002) Beryllium minerals and Be in rock-forming minerals in metamorphic environments. In: Grew ES (ed) Beryllium: mineralogy, petrology, and geochemistry. Mineral Soc Am Rev Mineral 50 (in press)

Grew ES, Hinthorne JR, Marquez N (1986) Li, Be, B, and Sr in margarite and paragonite from Antarctica. Am Mineral 71:1129–1134

Grew ES, Yates MG, Huijsmans JP, McGee JJ, Shearer CK, Wiedenbeck M, Rouse R (1998) Werdingite, a borosilicate new to granitic pegmatites. Can Mineral 36:399–414

Guggenheim S (1984) The brittle micas. In: Bailey SW (ed) Micas. Mineral Society Am Rev Mineral 13:257–298

Harley SL (1994) Cordierite as a sensor of fluid and melt distribution in crustal metamorphism. Mineral Mag 58A:374–375

Harley SL, Carrington DP (2001) The distribution of H_2O between cordierite and granitic melt; H_2O incorporation in cordierite and its application to high-grade metamorphism and crustal anatexis. J Petrol 42:1595–1620

Harley SL, Thompson P, Buick I (2002) Cordierite volatile contents and the role of post-peak metamorphic reactions. Int Mineral Assoc Programme Abstr 18:MH4, 205

Hensen BJ, Green DH (1973) Experimental study of the stability of cordierite and garnet in pelitic compositions at high pressures and temperatures. III. Synthesis of experimental data and geological applications. Contrib Mineral Petrol 38:151–166

Hervig RL (2002) Beryllium analyses by secondary ion mass spectrometry. In: Grew ES (ed) Beryllium: mineralogy, petrology, and geochemistry. Mineral Soc Am Rev Mineral 50 (in press)

Hinton RW (1999) NIST SRM 610, 611 and SRM 612, 613 multi-element glasses; constraints from element abundance ratios measured by microprobe techniques. Geostand Newslett 23:197–207

Hölscher A, Schreyer W (1989) A new synthetic hexagonal BeMg-cordierite, $Mg_2[Al_2BeSi_6O_{18}]$, and its relationship to Mg-cordierite. Eur J Mineral 1:21–37

Holtz F, Behrens H, Dingwell DB, Johannes W (1995) H_2O solubility in haplogranitic melts; compositional, pressure, and temperature dependence. Am Mineral 80:94–108

Holtz F, Scaillet B, Behrens H, Schulze F, Pichavant M (1996) Water contents of felsic melts; application to the rheological properties of granitic magmas. In: Brown M, Candela PA, Peck DL, Stephens WE, Walker RJ, Zen E (eds) Proc 3rd Hutton

Symp The Origin of Granites and Related Rocks. Geol Soc Am Spec Pap 315:57–64
Huebner JS (1971) Buffering techniques for hydrostatic systems at elevated pressures. In: Ulmer GC (ed) Research techniques for high pressure and high temperature. Springer, Berlin Heidelberg New York, pp 123–177
Icenhower JP (1995) Experimental determination of element behavior in silicic systems during hydrous partial fusion. PhD Thesis, University of Oklahoma, Norman
Icenhower JP, London D (1995) An experimental study of element partitioning among biotite, muscovite, and coexisting peraluminous silicic melt at 200 MPa (H_2O). Am Mineral 80:1229–1251
Icenhower JP, London D, Layne GD (1994) Element partitioning among biotite, muscovite, garnet, cordierite, and peraluminous melt: behavior of Li and Mn. Geol Soc Am Abstr Programs 26(7):290
Kalt A, Berger A, Blumel P (1999) Metamorphic evolution of cordierite-bearing migmatites from the Bayerische Wald (Variscan Belt, Germany). J Petrol 40:601–627
Kamber BS, Frei R, Gibb AJ (1998) Pitfalls and new approaches in granulite chronometry: an example from Limpopo Belt, Zimbabwe. Precambrian Res 91:269–285
Kennan P (2001) The S-type Leinster granite in SE Ireland. In: Chappell B, Fleming P (eds) S-type granites and related rocks. Abstr Aust Geol Surv Org Rec 2001/02:65–66
Kirchner D, Mirwald PW, Schreyer W (1984) Experimenteller Li-Einbau in Mg-Cordierit. Fortschritt Mineral Beih 62:119–120
Kretz R, Loop J, Hartree R (1989) Petrology and Li-Be-B geochemistry of muscovite-biotite granite and associated pegmatite near Yellowknife, Canada. Contrib Mineral Petrol 102:174–190
Kriegsman LM, Hensen BJ (1998) Back reaction between restite and melt: implications for geothermobarometry and pressure-temperature paths. Geology 26:1111–1114
Linnen RL, Pichavant M, Holtz F (1996) The combined effects of f_{O2} and melt composition on SnO_2 solubility and tin diffusivity in haplogranitic melts. Geochim Cosmochim Acta 60:4965–4976
Lofgren GE (1983) Effect of heterogeneous nucleation on basaltic textures: a dynamic crystallization study. J Petrol 24:229–255
London D (1995) Geochemical features of peraluminous granites, pegmatites, and rhyolites as sources of lithophile metal deposits. In: Thompson JFH (ed) Magmas, fluids, and ore deposits. Mineral Assoc Can Short Course 23:175–202
London D, Evensen JM (2002) Beryllium in silicic magmas and the origin of beryl-bearing pegmatites. In: Grew ES (ed) Beryllium: mineralogy, petrology, and geochemistry. Mineral Soc Am Rev Mineral 50 (in press)
London D, Wolf MB, Morgan GM, Gallegos Garrido M (1999) Experimental silicate-phosphate equilibria in peraluminous granitic magmas, with a case study of the Albuquerque Batholith at Tres Arroyos, Badajoz, Spain. J Petrol 40:215–240
Luecke W (1981) Lithium pegmatites in the Leinster Granite (southeast Ireland). Chem Geol 34:195–233
Marsh BD (1996) Solidification fronts and magmatic evolution. Mineral Mag 60:5–40
Miller CF, Bradfish LJ (1980) An inner Cordilleran belt of muscovite-bearing plutons. Geology 8:412–416
Morgan GB, London D (1996) Optimizing the electron microprobe of hydrous alkali aluminosilicate glasses. Am Mineral 81:1176–1185
Morgan GB, London D, Luedke R (1998) The late-Miocene peraluminous silicic volcanics of the Morococala field, Bolivia. J Petrol 39:601–632
Mukhopadhyay B, Holdaway MJ (1994) Cordierite-garnet-sillimanite-quartz equilibrium. I. New experimental calibration in the system FeO-Al_2O_3-SiO_2-H_2O and certain P-T-X_{H2O} relations. Contrib Mineral Petrol 116:462–472
Neiva ANR, Neiva JMC, Parry SJ (1987) Geochemistry of the granitic rocks and their minerals from Serra da Estrela, central Portugal. Geochim Cosmochim Acta 51:439–454
Norton JJ, Redden JA (1990) Relations of zoned pegmatites, granites, and metamorphic rocks in the southern Black Hills, South Dakota. Am Mineral 75:631–655
Ottolini L, Bottazzi P, Vannucci R (1993) Quantification of lithium, beryllium, and boron in silicates by secondary ion mass spectrometry using conventional energy filtering. Anal Chem 65:1960–1968
Pan Y, Breaks FW (1997) Rare-elements in fluoroapatite, Separation Lake Area, Ontario: evidence for S-type granite – rare-element pegmatite linkage. Can Mineral 35:659–671
Patiño Douce AE (1992) Calculated relationships between activity of alumina and phase assemblages of silica-saturated igneous rocks: petrogenetic implications of magmatic cordierite, garnet and aluminosilicate. J Volcanol Geotherm Res 52:43–63
Peacor DR, Wedepohl KH (1978) Manganese. In: Wedepohl KH (ed) Handbook of geochemistry, vol II(3). Springer, Berlin Heidelberg New York, pp 25-A-1–25-O-2
Pearce NJG, Perkins WT, Westgate JA, Gorton MP, Jackson SE, Neal CR, Chenery SP (1997) A compilation of new and published major and trace-element data for NIST SRM 610 and SRM 612 glass reference materials. Geostand Newslett 21:115–144
Pereira MD, Bea F (1994) Cordierite-producing reactions in the Peña Negra Complex, Avila Batholith, Central Spain. Can Mineral 32:763–780
Pouchou JL, Pichoir F (1985) "PAP" (ϕ-ρ-Z) correction procedure improved quantitative microanalysis. In: Armstrong JT (ed) Microbeam analysis. San Francisco Press, pp 104–106
Raimbault L, Cuney M, Azencott C, Duthou JL, Joron JL (1995) Geochemical evidence for a multistage magmatic genesis of Ta-Sn-Li mineralization in the granite at Beauvoir, French Massif Central. Econ Geol Bull Soc Econ Geol 90:548–576
Ramirez JA, Grundvig S (2000) Causes of geochemical diversity in peraluminous granitic plutons: the Jalmala pluton, Central-Iberian Zone (Spain and Portugal). Lithos 50:171–190
Russ JC (1999) The image processing handbook, 3rd edn. CRC Press, Boca Raton
Schreyer W, Gordillo CE, Werding G (1979) A new sodium–beryllium cordierite from Soto, Argentina, and the relationship between distortion index, Be content, and state of hydration. Contrib Mineral Petrol 70:925–946
Schreyer W, Maresch WV, Daniels P, Wolsdorff P (1990) Potassic cordierites: characteristic minerals for high-temperature, very low pressure environments. Contrib Mineral Petrol 105:162–172
Secchi FA, Brotzu P, Callegari E (1991) The Arbruse igneous complex (SW Sardinia, Italy) – an example of dominant igneous fractionation leading to peraluminous cordierite-bearing leucrogranites as residual melts. Chem Geol 92:213–249
Shearer CK, Papike JJ, Laul JC (1987) Mineralogical and chemical evolution of a rare-element granite–pegmatite system; Harney Peak Granite, Black Hills, South Dakota. Geochim Cosmochim Acta 51:473–486
Silver LA, Stolper EM (1989) Water in albitic glasses. J Petrol 30:667–709
Smeds SA (1992) Trace-element in potassium-feldspar and muscovite as a guide in the prospecting for lithium- and tin-bearing pegmatites in Sweden. J Geochem Explor 42:351–369
Spear FS, Cheney JT (1989) A petrogenetic grid for pelitic schists in the system SiO_2-Al_2O_3-FeO-MgO-K_2O-H_2O. Contrib Mineral Petrol 101:149–164
Thompson P, Harley SL, Carrington DP (2002) Sodium and potassium in cordierite – a potential thermometer for melts? Eur J Mineral 14:459–470
Turekian KK, Wedepohl KH (1961) Distribution of the elements in some major units of the Earth's crust. Geol Soc Am Bull 72:175–191
Ugidos JM (1988) New aspects and considerations on the assimilation of cordierite-bearing rocks. Rev Soc Geol Esp 1:129–133

Ugidos JM (1990) Granites in the Central Iberian Massif as a paradigm of genetic processes of granitic rocks: I-types vs S-types. In: Dallmayer RD, Martínez Garcia E (eds) Pre-Mesozoic geology of Iberia. Springer, Berlin Heidelberg New York, pp 189–206

Ugidos JM, Recio C (1993) Origin of cordierite-bearing granites by assimilation in the Central Iberian Massif (CIM), Spain. Contrib Mineral Petrol 103:27–43

Vielzeuf D, Holloway JR (1988) Experimental determination of the fluid-absent melting relations in the pelitic system. Contrib Mineral Petrol 98:257–276

Watson EB, Capobianco CJ (1981) Phosphorus and the rare earth elements in felsic magmas: An assessment of the role of apatite. Geochim Cosmochim Acta 45:2349–2358

White AJR, Clemens JD, Holloway JR, Silver LT, Chappell BW, Wall VJ (1986a) S-type granites and their probable absence in southwestern North America. Geology 14:115–118

White AJR, Clemens JD, Holloway JR, Silver LT, Chappell BW, Wall VJ (1986b) Reply to C.F. Miller's comment on S-type granites and their probable absence in southwestern North America. Geology 14:805–806

Wolf MB, London D (1994) Apatite dissolution into peraluminous haplogranitic melts: an experimental study of solubilities and mechanisms. Geochim Cosmochim Acta 58:4127–4145

Wolf MB, London D (1997) Boron in granitic magmas: stability of tourmaline in equilibrium with biotite and cordierite. Contrib Mineral Petrol 130:12–30

Wuensch BJ, Hörmann PK (1978) Beryllium. In: Wedepohl KH (ed) Handbook of geochemistry, vol II(1). Springer, Berlin Heidelberg New York, pp 4-A-1–4-O-1

You CF, Morris JD, Gieskes JM, Rosenbauer R, Zheng SH, Xu X, Ku TL, Bischoff JL (1994) Mobilization of beryllium in the sedimentary column at convergent margins. Geochim Cosmochim Acta 58:4887–4897

Zen E (1987) Wet and dry AFM assemblages of peraluminous granites and the usefulness of cordierite as the prime indicator of S-type granite. Geol Soc Am Abstr Programs 19:904